Andean Geology 37 (1): 144-176. January, 2010

Andean Geology
formerly Revista Geológica de Chile
www.scielo.cl/andgeol.htm

Geochronological and thermochronological constraints on porphyry copper mineralization in the Domeyko alteration zone, northern Chile

Víctor Maksaev[1], Tomás A. Almonacid[2], Francisco Munizaga[1], Víctor Valencia[3], Michael McWilliams[4], Fernando Barra[3]

[1] *Departamento de Geología, Universidad de Chile, Casilla 13518, Correo 21, Santiago, Chile. vmaksaev@ing.uchile.cl; fmunizag@ing.uchile.cl*

[2] *Minera Peñoles de Perú S.A., Av. Central No. 643 Of. 201, San Isidro, Lima, Perú. Tomas_Almonacid@penoles.com.mx*

[3] *Department of Geosciences, University of Arizona, 1040 E. 4th Street, Bldg. #77, Tucson, AZ 85721, USA. victorv@email.arizona.edu; fbarra@email.arizona.edu*

[4] *CSIRO Exploration and Mining, 26 Dick Perry Avenue, Kensington WA 6151, Australia; PO Box 1130, Bentley WA 6102, Australia. Mike.Mcwilliams@csiro.au*

ABSTRACT. At Domeyko, 40 km south of Vallenar in northern Chile (28°57'S-70°53'W), the Dos Amigos and Tricolor porphyry copper centers are located within a north-south-elongated hydrothermal alteration zone 6x1.5 km of surface dimensions. The centers are related to tonalite to granodiorite porphyry stocks displaying potassic alteration, which are surrounded by Lower Cretaceous andesitic volcanic rocks with sericitic, kaolinite-illite and propylitic alteration zones. The western boundary of the alteration zone is marked by the post-mineralization Cachiyuyo Batholith of granodioritic to dioritic composition. U-Pb zircon ages for the Dos Amigos porphyry are of 106.1±3.5 and 104.0±3.5 Ma; and 108.5±3.4 for the nearby Tricolor porphyry. The Cachiyuyo Batholith yielded U-Pb zircon ages of 99.6±1.8 and 99.1±1.9 Ma; and $^{40}Ar/^{39}Ar$ ages for biotite of 96.9±3.9 and 94.8±0.9 Ma. These dates indicate that batholith emplacement postdated the Dos Amigos and Tricolor porphyries, in agreement with geological relationships. Although copper mineralization is spatially and genetically related to the Lower Cretaceous (Albian) porphyry stocks, most of the dated hydrothermal micas from the Dos Amigos and Tricolor porphyries yielded $^{40}Ar/^{39}Ar$ ages between 97.1±2.5 and 96.0±1.4 Ma, which overlap within error with the cooling ages obtained for the neighboring batholith. $^{40}Ar/^{39}Ar$ dating of micas revealed significant disturbance of their K-Ar isotopic systematics that complicates accurate determination of the timing of hydrothermal activity at Domeyko. Nevertheless, the $^{40}Ar/^{39}Ar$ data establish a minimum Late Cretaceous age for this activity. A fission track age of 59.8±9.8 Ma of apatite from the Dos Amigos porphyry indicates cooling through the temperature range of the apatite partial annealing zone (~125-60°C) during the Paleocene; and an (U-Th)/He age of 44.7±3.7 Ma of apatite from the same porphyry sample shows cooling through the temperature range of the apatite He partial retention zone (~85-40°C) during the Eocene. These ages correspond to the exhumation of the porphyry, and the latter provides a maximum age for the supergene enrichment processes that formed the chalcocite blanket currently mined at Dos Amigos.

Keywords: Porphyry copper, Andes, Chile, Geochronology, Thermochronology, Coastal Cordillera.

RESUMEN. Determinaciones geocronológicas y termocronológicas para la mineralización de cobre porfídico en la zona de alteración de Domeyko, norte de Chile. En Domeyko, a 40 km al sur de la ciudad de Vallenar, en el norte de Chile (28°57'S-70°53'O), se ubican los pórfidos cupríferos Dos Amigos y Tricolor dentro de una zona de alteración hidrotermal elongada en sentido norte-sur de 6x1,5 km. Estos están relacionados con stocks porfídicos tonalíticos a granodioríticos con alteración potásica, rodeados por zonas de alteraciones sericítica, caolinita-illita y propilítica, las cuales afectaron principalmente rocas volcánicas del Cretácico Inferior. El límite oeste de la zona de alteración lo constituye el Batolito Cachiyuyo postmineral de composición granodiorítica a diorítica. Edades U-Pb en circón para el pórfido Dos Amigos son de 106,1±3,5 Ma y 104,0±3,5 Ma y de 108,5±3,4 Ma para el pórfido Tricolor. El Batolito Cachiyuyo adyacente dio edades U-Pb en circón de 99,6±1,9 y 99,1±1,9 Ma y edades $^{40}Ar/^{39}Ar$ en biotita de 96,9±3,9 y 94,8±0,9 Ma. De acuerdo a estas edades el emplazamiento del batolito fue posterior a los pórfidos Dos Amigos y Tricolor, consistente con las relaciones geológicas. Aunque la mineralización de cobre está relacionada espacialmente y genéticamente con los stocks porfídicos del Cretácico Inferior (Albiano), la mayoría de las micas datadas de los pórfidos Dos Amigos y Tricolor dieron edades $^{40}Ar/^{39}Ar$ entre 97,1±2,5 y 96,0±1,4 Ma, las cuales son coincidentes con las edades de enfriamiento obtenidas para el batolito. La datación $^{40}Ar/^{39}Ar$ por pasos de micas reveló una importante perturbación del sistema isotópico K-Ar de las mismas, lo que complica una determinación exacta de la edad de la actividad hidrotermal en Domeyko, pero los datos $^{40}Ar/^{39}Ar$ establecen con certeza una edad mínima Cretácico Tardío para ella. Una edad de trazas de fisión en apatita de 59,8±9,8 Ma para el pórfido Dos Amigos indica enfriamiento a través del rango de temperatura de la zona de acortamiento parcial de trazas en apatita (~125-60°C) durante el Paleoceno y una edad (U-Th)/He en apatita de 44,7±3,7 Ma obtenida para el mismo pórfido revela enfriamiento a través del rango de la zona de retención parcial de He en apatita (~85-40°C) durante el Eoceno. Estas edades corresponden a la exhumación del pórfido y la última provee una edad máxima para los procesos de enriquecimiento supérgeno que formaron el nivel enriquecido con calcosina actualmente en explotación en la mina Dos Amigos.

Palabras clave: Pórfido cuprífero, Andes, Chile, Geocronología, Termocronología, Cordillera de la Costa.

1. Introduction

The Domeyko alteration zone is located in the southern part of the Atacama Desert, 40 km south of Vallenar (28°57'S-70°53'W; Fig. 1). It includes the Dos Amigos porphyry copper deposit, currently being exploited, and the Tricolor porphyry copper occurrence (Fig. 2). Regionally, these deposits are part of a Mid-Late Cretaceous belt of porphyry copper deposits that extends along the eastern flank of the Coastal Cordillera of northern Chile, between latitudes 26° and 31°S (Llaumett, 1975; Camus, 2002, 2003; Sillitoe and Perelló, 2005; Maksaev *et al*., 2006a, 2007) (Fig. 3).

The Domeyko alteration zone was first explored for its porphyry copper potential from 1962 to 1964, during a 'Program for Development' funded by the United Nations (Kents, 1962[1]), which detected copper mineralization occurrences at Tricolor and Dos Amigos (Fig. 2);

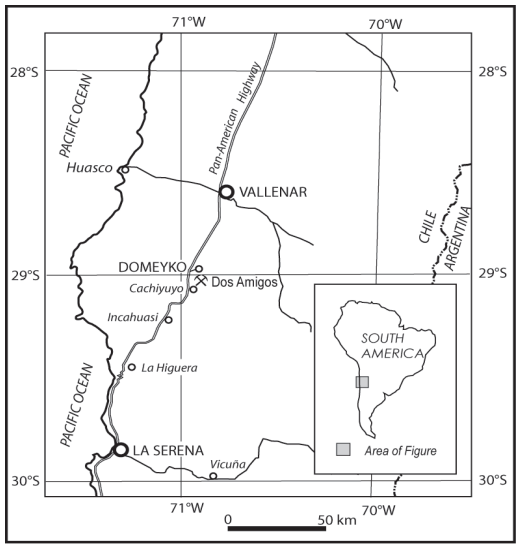

FIG. 1. Location map of Domeyko mining village and the Dos Amigos mine complex.

[1] Kents, P. 1962. Domeyko hydrothermal development, Department Chañaral, Province of Atacama (unpublished report), United Nations Special Fund: 6 p.

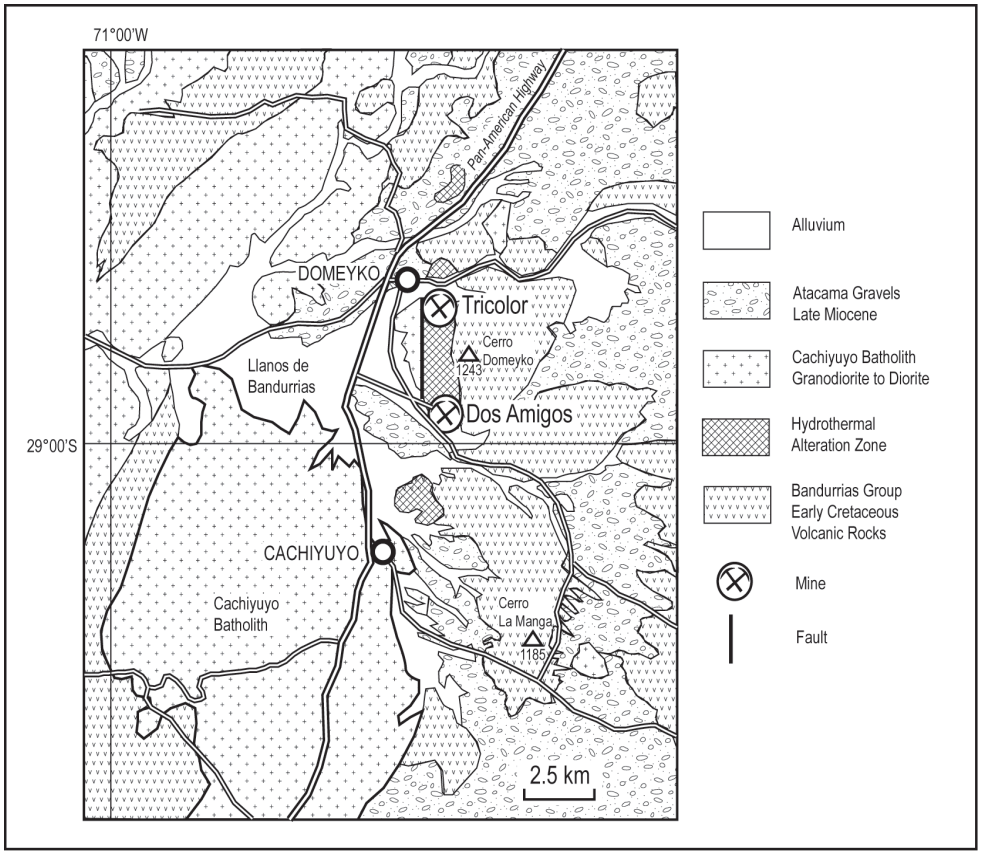

FIG. 2. Geological setting of the Domeyko alteration zone and the Dos Amigos and Tricolor porphyry copper centers. Regional geology modified after Moscoso *et al*. (1982).

six drill holes (totaling 683 m) were completed at Tricolor intercepting low-grade hypogene copper intervals between 0.13 to 0.32 percent. It was followed by exploration during the years 1968 to 1971 by the governmental institution 'Corporación Nacional de Fomento' (CORFO) in the Dos Amigos area, including 43 diamond drill holes (totaling 5,361 m) and 4 percussion drill holes (236 m). This program identified a supergene copper enrichment zone for which a resource of 3.5 million metric tons averaging 1.18 percent copper was estimated (Palafox, 1975[2]). Further exploration at Dos Amigos by Shell Chile between 1982 and 1983 expanded the supergene resource to 5 million metric tons at about 1 percent copper and 0.25 grams per metric ton gold and discovered additional hypogene mineralization of 36 million metric tons at 0.36 percent copper and 0.26 grams per ton gold. Since 1996, the enrichment blanket at Dos Amigos has been the objective of open pit mining by Compañía Explotadora de Minas (CEMIN), with annual average extraction of 1 million ton of ore averaging 1 percent copper, which is processed by heap leaching and solvent extraction-electrowinning (SX/EW) methods.

There are no previous publications on the geology of the Domeyko alteration zone, except for two whole rock K-Ar determinations of 106±10 and 97±20 Ma for altered rocks reported by Munizaga *et al*. (1985). Consequently, the present contribution constitutes the first geological

[2] Palafox, L. 1975. 'María Soledad', Domeyko, Atacama, Chile. Property Examination Report (unpublished report), COMINCO Ltd. Exploration: 9 p.

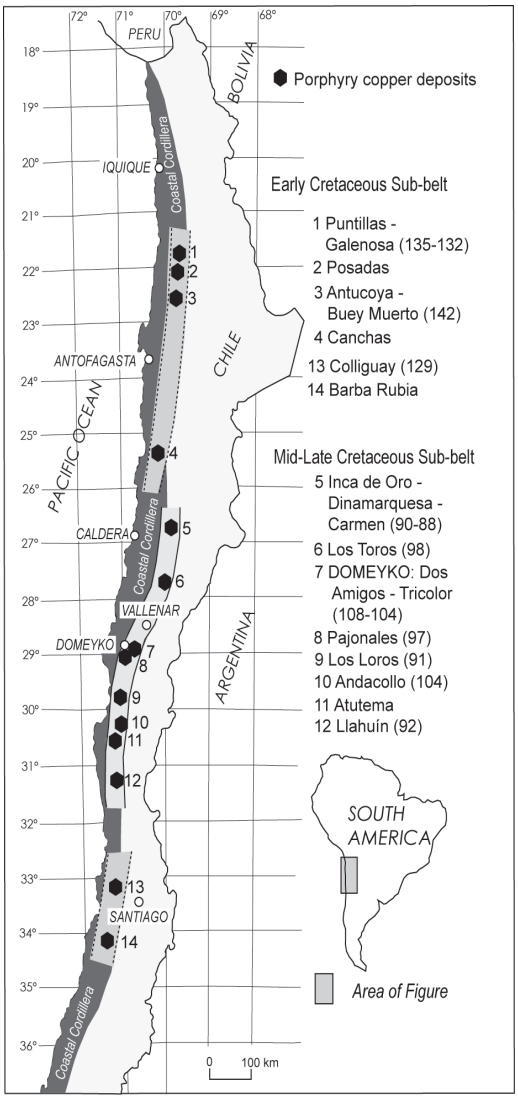

FIG. 3. The Cretaceous porphyry copper belt of northern Chile. Ages of deposits compiled from Camus (2003), Sillitoe and Perelló (2005) and Maksaev *et al.* (2006b).

description of the area. It provides new U-Pb, $^{40}Ar/^{39}Ar$, fission track and (U-Th)/He data that confirm its position within a mid-Cretaceous metallogenic episode of porphyry copper mineralization (*e.g.*, Sillitoe and Perelló, 2005). The present work also provides a time-temperature model for the low-temperature cooling of the Dos Amigos porphyry, which in turn helps to constrain the timing of the supergene processes and associated chalcocite enrichment.

2. Metallogenic setting

The porphyry copper belt that extends along the eastern flank of the Coastal Cordillera of northern Chile was initially recognized as the 'Pacific Belt' of Chilean porphyry copper deposits by Llaumett (1975). Subsequent geochronological work has shown that the porphyry copper systems located between latitudes 21° and 23°S form a sub-belt with ages from 142 to 132 Ma (Munizaga *et al*., 1985; Reyes, 1991; Boric *et al*., 1990; Perelló *et al*., 2003; Sillitoe and Perelló, 2005; Maksaev *et al*., 2006a); this belt seems to re-appear south of latitude 33°S (Fig. 3), but there are insufficient geochronological data to prove it. The porphyry copper deposits and prospects located in the Coastal Cordillera between latitudes 26° and 31°S form another sub-belt with U-Pb ages from 108 to 88 Ma (Maksaev *et al*., 2006b) (Fig. 3). The largest historic and current copper producer of the last sub-belt is the Andacollo porphyry copper-gold deposit (Llaumett *et al*., 1975; Reyes, 1991). It has been operated since 1996 by the Compañía Minera Carmen de Andacollo (ownership: 90% Teck and 10% 'Empresa Nacional de Minería'), with an average annual production of 21,000 tons cathode copper. Open pit mining at Andacollo to date has exclusively concentrated on leachable resources amounting to 34.6 million metric tons of 0.73 percent copper in the supergene chalcocite enrichment blanket, but its hypogene zone with resources of 311 million metric tons averaging 0.46 percent copper and 0.15 grams per ton gold is currently being prepared for production. In addition to the production at Dos Amigos deposit, a number of the other porphyry copper prospects from the sub-belt have been explored to varying degree, but have not attained production status (*e.g.*, Los Toros, Los Loros; Fig. 3). In general, the Cretaceous porphyry deposits of the Coastal Cordillera are much smaller (resources <~300 million metric tons) and possess lower hypogene grades (<0.4% Cu) than those of the Cenozoic porphyry copper belts located farther east and at higher elevations in the Chilean Andes (*e.g.*, Sillitoe and Perelló, 2005). The Cretaceous deposits are related to small stocks of quartz diorite to granodiorite porphyry emplaced into arc-related plutonic and volcanic rocks. They tend to be dominated by potassic alteration (biotite, K-feldspar) with a variably developed intermediate argillic overprint (illite, and/or smectite, chlorite, sericite). In addition, sericitic alteration is present at Andacollo, Antucoya-Buey Muerto, and in the

Domeyko alteration zone (Reyes, 1991; Perelló *et al*., 2003; Maksaev *et al*., 2006a).

During the Jurassic to Early Cretaceous a subduction-related magmatic arc developed along the area of the Coastal Cordillera in westernmost Chile. The arc was flanked eastward (inland) by a sedimentary-marine back-arc basin represented by carbonate strata of the Chañarcillo Group (Segerstrom and Parker, 1959; Moscoso *et al*., 1982; Arévalo *et al*., 2005; Arévalo, 2005a, b). The porphyry copper sub-belt with U-Pb ages from 108 to 88 Ma extends along the eastern edge of this magmatic arc. The copper deposits were formed during and after the mid-Cretaceous (Albian) tectonic inversion of the back-arc basin, as shown by the end of marine sedimentation of the Chañarcillo Group and the onset of coarse-grained alluvial sedimentation and subaerial volcanism of the Cerrillos Formation during the late Aptian (*e.g*., Marschik and Fonboté, 2001; Marschik and Söllner, 2006; Charrier *et al*., 2007; Maksaev *et al*., 2009). This abrupt change in the sedimentary environment represents a significant modification of the tectonic regime on the continental margin from tensional to compressive (Maksaev *et al*., 2009), in turn related to a major reorganization of the Andean orogen involving the closure of the back-arc basins all along the western margin of South America (Dalziel, 1986; Bourgois *et al*., 1987; Mpodozis and Ramos, 1990).

This porphyry copper sub-belt runs parallel to, but some 10-15 km to the east of the 'Chilean Iron Belt' (Ruiz *et al*., 1965) made of a number of iron oxide-apatite and iron oxide-copper-gold deposits distributed along the southernmost segment (26°-30°S) of the Atacama Fault Zone (Fig. 4) (Ruiz *et al*., 1965; Espinoza, 1990; Nyström and Henríquez, 1994; Sillitoe, 2003; Gelcich *et al*., 2005; Maksaev *et al*., 2007). The Atacama Fault Zone is a major sinistral, strike-slip fault system that extends along the Coastal Cordillera for more than 1,000 km between latitudes 20° and 30° (Arabasz, 1971; Scheuber and González, 1999) (Fig. 4). It developed in the Jurassic with sinistral shear persisting into the Early Cretaceous in an overall transtensional tectonic setting along the magmatic arc, in close association with regional pluton emplacement, as well as crustal thinning and subsidence (Taylor *et al*., 1998; Brown *et al*., 1993; Dallmeyer *et al*., 1996; Scheuber and Andriessen, 1990; Scheuber *et al*., 1995; Scheuber and Gonzalez, 1999; Grocott and Taylor, 2002). K-Ar and $^{40}Ar/^{39}Ar$ ages for actinolite from magnetite-apatite deposits

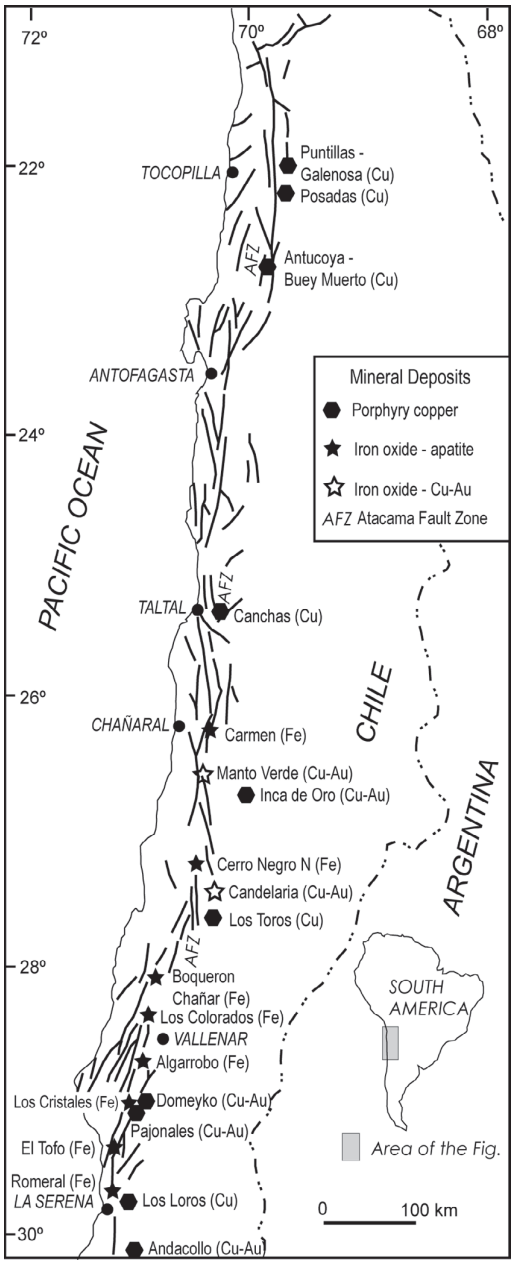

FIG. 4. The spatial relationship of the Cretaceous iron oxide-apatite deposits of the Chilean Iron Belt, iron oxide copper-gold and the Lower Cretaceous porphyry copper deposits with major faults of the Atacama Fault Zone (AFZ) along the Coastal Cordillera of Northern Chile. Modified after Brown *et al*. (1993), Vila *et al*. (1996) and Maksaev and Zentilli (2002).

of 129 to 96 Ma have been published (*e.g*., Munizaga *et al*., 1985; Oyarzún *et al*., 2003; Díaz *et al*.,

2003) and suggest chronological overlapping with the 108 to 88 Ma range of the porphyry copper sub-belt. However, older and more accurate U-Pb ages for magnetite and apatite from 131 to 127 Ma have also been reported for deposits of the Chilean Iron Belt (Gelcich *et al*., 2005). Therefore, the deposits of the Chilean Iron Belt represent a metallogenic episode that preceded in time the formation of the porphyry copper deposits. Whole-rock K-Ar ages of of 117±3 and 121±3 Ma for altered andesites and dykes at Manto Verde were initially taken to indicate the age of the primary mineralization of iron oxide-copper-gold deposits (Vila *et al*., 1996), but more precise U-Pb ages of 128.9±0.6 and 126.4±0.5 Ma for a quartz monzonite to granodioritic dyke with potassic alteration, led Gelcich *et al*. (2003) to conclude that mineralization at Manto Verde is most probably even older. Likewise, dates older than those of the porphyry copper sub-belt have been reported for the Candelaria iron oxide-copper-gold deposit, including Re/Os molybdenite dates of 114.2±0.6 and 115.2±0.6 Ma interpreted as mineralization ages by Mathur *et al*. (2002). These are coincident with the 115.1±0.2 Ma $^{40}Ar/^{39}Ar$ plateau age for biotite associated with chalcopyrite–pyrite reported by Marschik and Fontboté (2001) and the $^{40}Ar/^{39}Ar$ plateau ages of 114.2±0.8 and 114.1± 0.7 Ma for biotite of Ullrich & Clark (1999). However, a younger $^{40}Ar/^{39}Ar$ plateau age of 111.7±0.8 Ma for amphibole (Ullrich and Clark, 1999) and similar $^{40}Ar/^{39}Ar$ ages of 111.0±1.7 and 110.7±1.6 Ma for biotite (Arévalo *et al*., 2006) probably represent a later event of alteration at Candelaria, which overlaps within error with the oldest ages of the porphyry sub-belt. Thus, it is possible that mineralization at Candelaria represents a transition between iron oxide-copper-gold and porphyry copper metallogenic events during the mid-Cretaceous basin inversion along the Coastal Cordillera of northern Chile between latitudes 26° and 31°S.

3. Local Geology

The Domeyko alteration zone is located in a region characterized by rolling hills and intermontane depressions at an average elevation of 800 m. It is exposed along a ridge that rises to 1243 m in elevation at the Domeyko hill, with dimensions of 6 km in the NS direction and 1 to 1.5 km in the EW direction (Fig. 2). The ridge stands above relics of extensive west-sloping terraces of Miocene gravels formed by coalescent alluvial fans, developed at elevations between 950 and 780 m (Atacama Gravels; Mortimer, 1973; Moscoso *et al*., 1982).

An unaltered, granodioritic to dioritic batholith (herein referred to as the Cachiyuyo Batholith) constitutes the abrupt western boundary of the Domeyko alteration zone. The batholith intruded the altered volcanic rocks, but its contact also coincides locally with a north-trending regional fault (Fig. 2). The majority of the altered rocks are part of a NNW-striking and E-dipping succession of Neocomian age assigned to the Bandurrias Group (Moscoso *et al*., 1982) and composed of andesitic lavas and volcanic breccias, with subordinate dacite. Minor intrusive bodies and dikes of fine-grained, green-colored andesite are emplaced in the volcanic succession.

Two porphyry stocks intrude the volcanic rocks at Tricolor and Dos Amigos (Figs. 3 and 5). The Dos Amigos porphyry is tonalitic to granodioritic in composition with plagioclase and quartz phenocrysts, up to 4 mm in diameter, in a microcrystalline groundmass composed of an aggregate of plagioclase and quartz; some plagioclase phenocryst margins display vermicular intergrowths with K-feldspar. The porphyry contains fine-grained hydrothermal biotite profusely disseminated and microcrystalline biotite aggregates replacing amphibole. The Tricolor porphyry is of similar composition with plagioclase and minor quartz phenocrysts in a microcrystalline groundmass composed of an aggregate of similar components. The porphyry contains abundant fine-grained opaque minerals and hydrothermal biotite profusely disseminated; the latter typically altered to chlorite.

A composite hydrothermal breccia body (Marisol breccia) is exposed over a surface area of 500x600 m immediately north of the Dos Amigos mine (Fig. 5); its central part is polymictic and matrix-support-ed, with sericitically-altered angular fragments of volcanic rocks and porphyry in a matrix (30-40%) of tourmaline and rock flour; abundant pyrite, but only minor chalcopyrite are visible in the breccia matrix in exploration adits. The marginal part of the Marisol breccia is formed by subrounded clasts of volcanic rocks in a matrix of silicified rock flour with sericite; underground this matrix includes pyrite. In an exploration adit 150 m beneath the surface, the breccia shows a higher proportion of strongly seriticized porphyry fragments in a matrix of tourmaline, pyrite, and quartz.

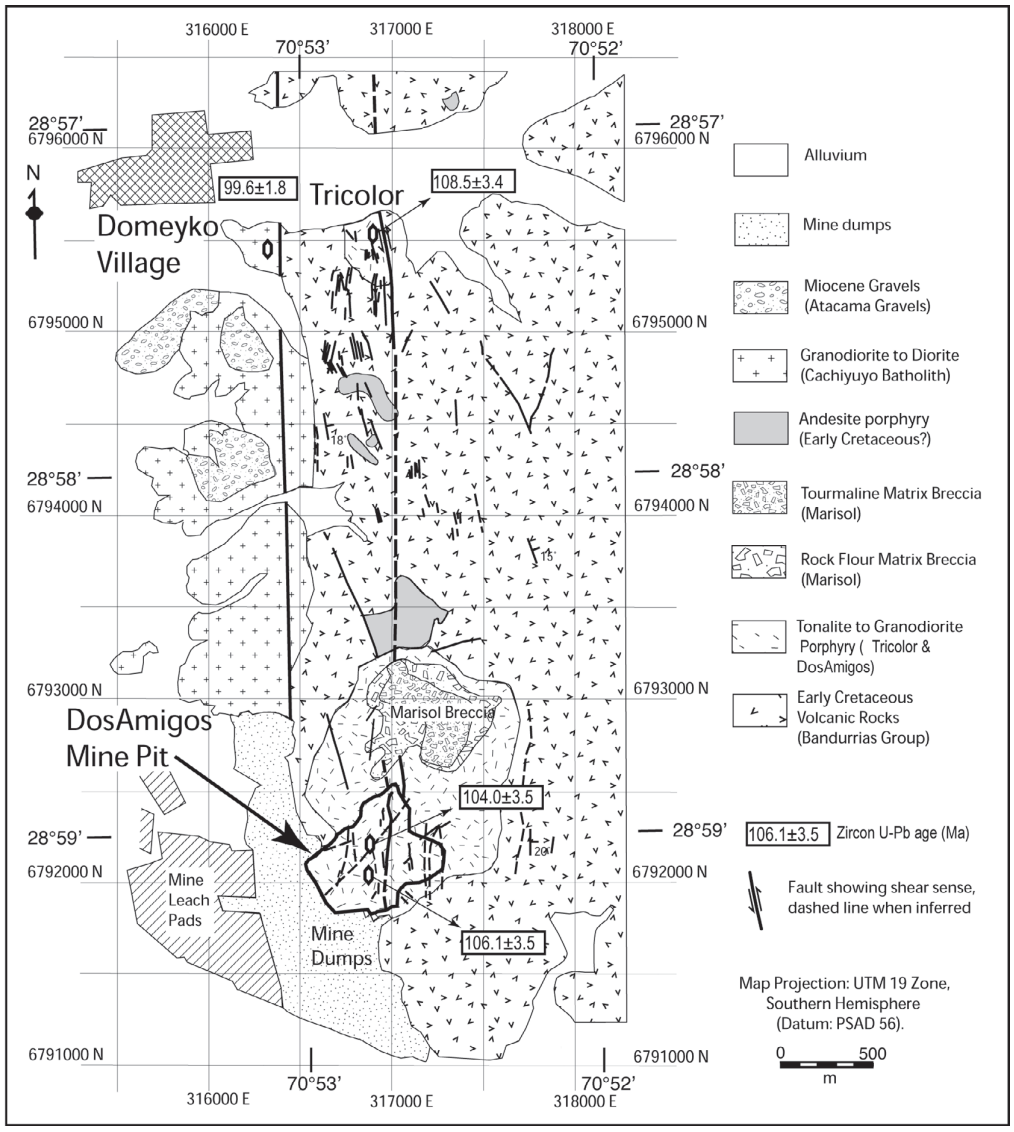

FIG. 5. Geological map of the Domeyko alteration zone showing the U-Pb zircon ages of intrusive rocks. Modified after Almonacid (2007).

A longitudinal fault zone traverses the whole altered area (Fig. 5), accompanied by a number of subsidiary northwest-trending subvertical faults; locally biotite-bearing porphyry is exposed at Tricolor with N-S/vertical foliation. The overall geometric fault pattern in the Domeyko alteration zone is compatible with a longitudinal sinistral shear (Almonacid, 2007).

3.1. Alteration types

The Domeyko alteration zone includes potassic, sericitic, kaolinite-illite, and propylitic alteration assemblages (Fig. 6). Potassic alteration is present at both Dos Amigos and Tricolor porphyries and in the immediately surrounding volcanic rocks east of Tricolor. The potassic zone at Dos Amigos is

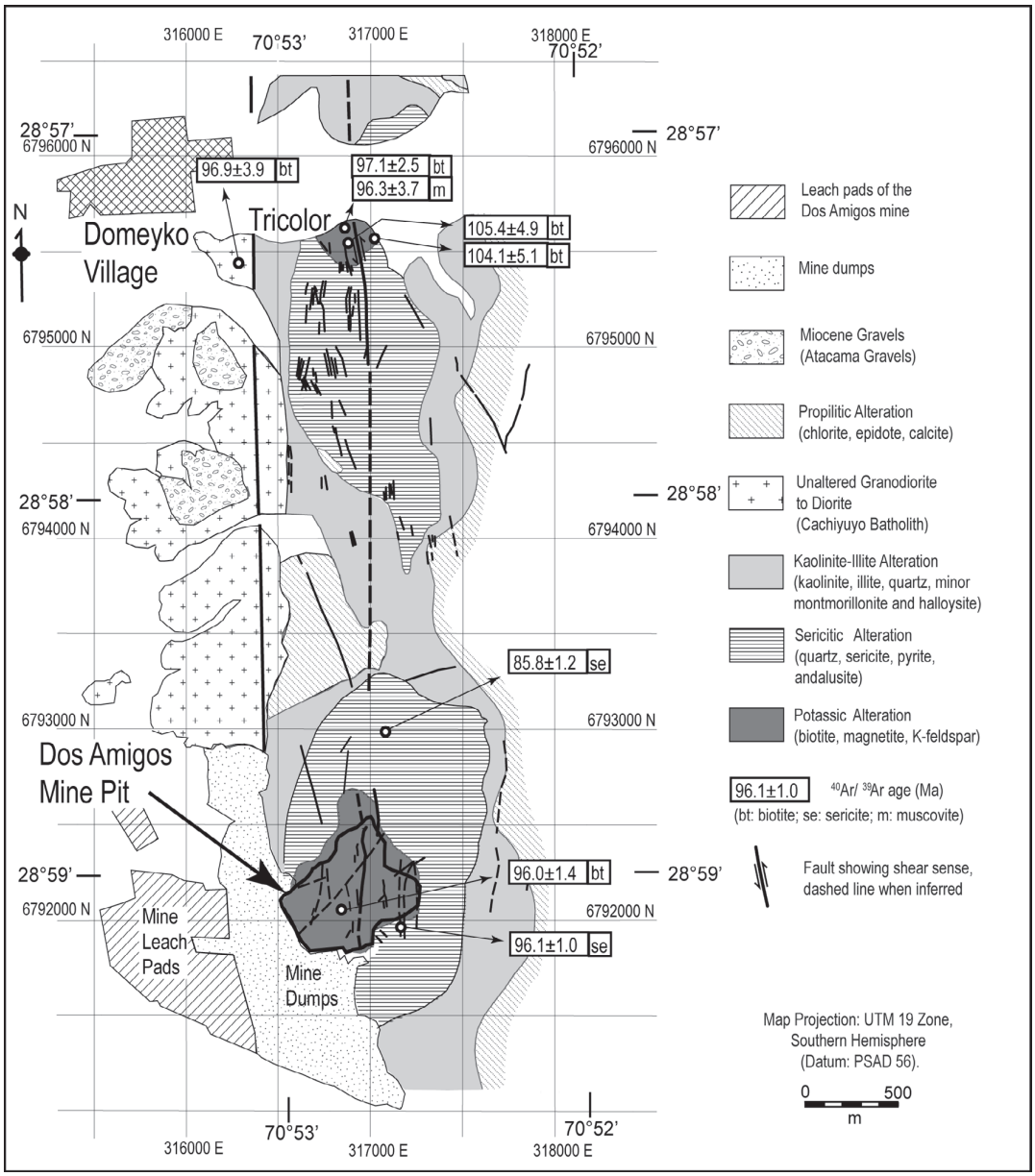

FIG. 6. Hydrothermal alteration map of the Domeyko alteration zone showing $^{40}Ar/^{39}Ar$ ages for micas. Modified after Almonacid (2007).

750x750 m in surface area, but that at Tricolor is only 250x250 m. The characteristic alteration mineral assemblage includes biotite and magnetite, with subordinate K-feldspar. The primary texture of the porphyries is largely preserved, but volcanic rocks adjacent to the porphyry at Tricolor are strongly biotitized, black in color and show texture obliteration. Sericitic alteration surrounds both potassic alteration centers; it is characterized by bleaching of the rocks, almost complete destruction of original rock texture and an assemblage of quartz, fine-grained white mica, pyrite, and minor andalusite. The sericitic zones grade

outward to rocks with preserved original texture, but with feldspars and mafic minerals altered to kaolinite, illite and quartz, with minor montmorillonite; this zone extends irregularly north-south for ~5 km. An external propylitic zone (chlorite, epidote and calcite) is mostly restricted to the eastern part of the Domeyko alteration zone (Fig. 6).

A supergene alteration overprint is apparent in most of the Domeyko alteration zone with common presence of halloysite and kaolinite, and fracture filling with supergene alunite and gypsum.

3.2. Mineralization

The Domeyko alteration zone exposes a leached cap characterized by the presence of profuse limonite staining and impregnation comprising goethite and hematite, which give an overall reddish color to the rocks of the area. This leached cap has an average thickness of 100 m over the Dos Amigos deposit and Marisol hydrothermal breccia body. A limited zone with oxidized copper minerals is preserved at the bottom of the leached cap at Dos Amigos; its thickness is irregular, ranging from a few meters to ~30 m within fault zones. The main copper-bearing oxidized minerals are chrysocolla, atacamite and minor brochantite, which are accompanied by goethite and minor amarantite. At Tricolor a number of small shafts and adits along NNW and NW-trending fracture zones, from 0.3 to 1.2 m wide, contain chrysocolla and minor chalcocite.

A supergene chalcocite-enriched blanket is developed at Dos Amigos between 740 and 800 m elevation, with an average thickness of ~30 m and up to 60 m in faults and fractured zones. Within this blanket black, sooty chalcocite has replaced the margins of pyrite and chalcopyrite grains. Minor covellite and digenite exist from the middle part to the bottom of the blanket, also mostly as fine coatings to pyrite, chalcopyrite and bornite, with covellite becoming increasingly abundant in the lowermost part of the enrichment zone. Although the supergene sulfides are largely restricted to rimming of the hypogene sulfides, the copper grade of the enrichment zone get to 1.25 percent, for an overall enrichment factor of up to 3 times the hypogene copper grade. However, the supergene enrichment within the Marisol hydrothermal breccia body averages copper grade of less than 0.5 percent, due to the lower hypogene grade of this unit (0.2%; Almonacid, 2007).

Hypogene copper-bearing minerals are mostly chalcopyrite and lesser bornite, within a stockwork of quartz veins hosted by the Dos Amigos porphyry displaying biotite-dominated potassic alteration exposed on the pit floor of the mine (740 m level); its vertical extent is currently unknown and copper grade typically averages less than 0.36 percent, according to CEMIN data. Irregular and discontinuous biotitic veins, 0.02 to 2 mm thick, are the earliest veins in the porphyry, and contain abundant magnetite, but lack sulfides. These veins are cut by wavy, irregular and discontinuous, quartz-bearing veins with biotite, 0.2 to 6 mm thick, which contain pyrite, chalcopyrite, bornite, and magnetite. Both vein sets are, in turn, cut by straight and continuous quartz-bearing veins; mostly composed of anhedral and euhedral quartz with either central or parallel bands of pyrite, chalcopyrite, and magnetite, together with minor bornite, biotite and sericite. Late veins are composed of pyrite, quartz and minor muscovite with sericitic alteration envelopes; only rare pyrite-chalcopyrite intergrowths exist in these late veins.

The potassic-altered tonalitic to granodioritic porphyry that crops out at Tricolor also displays a stockwork of sulfide-bearing quartz veins beneath the leach capping, which are apparent in the dumps of an exploration adit at 800 m elevation.

Gold mineralization at Dos Amigos and Tricolor is poorly constrained. However, limited surface sampling reveals anomalous values mostly less than 0.3 grams per ton (between 0.11 and 0.88 g/t Au) for porphyries displaying potassic alteration; similarly, assays for 22 samples have returned average molybdenum values of only 15 parts per million (Almonacid, 2007).

4. Geochronology

4.1. Analytical procedures

4.1.1. U-Pb dating

Zircon grains from the Dos Amigos tonalite porphyry, the granodiorite porphyry of the Tricolor area, and the unaltered granodiorite and diorite of the Cachiyuyo Batholith were dated by LA-ICP-MS U-Pb. The new U-Pb zircon geochronological results are summarized in Table 1, and are plotted with error bars (±2σ) in figures 7 and 8. The U-Pb analytical data are included in appendix A.

The analytical work was performed at the University of Arizona using the laser ablation ICP-

TABLE 1. SUMMARY OF LA-ICP-MS ZIRCON U-Pb AGES AND SAMPLE LOCATION.

Sample	U-Pb Age (Ma±2σ)	Rock Type	Location (geodetic) and UTM (datum PSAD56)	Comments
KP-08	108.5±3.4	Tonalitic porphyry	28°57'17.19"S-70°52'44.28"W (6795604N-316896E)-H 823 m	Tricolor porphyry; weighted mean of 25 analyzed spots.
KP-13	106.1±3.5	Granodioritic porphyry	28°59'10.62"S-70°52'47.06"W (6792032N-316864E)-H730 m	Dos Amigos porphyry from mine pit; weighted mean of 25 analyzed spots.
KP-14	104.0±3.5	Tonalitic porphyry	28°59'04.03"S-70°52'46.72"W (6792235N-316870 E)-H 730 m	DOS Amigos porphyry from mine pit; weighted mean of 24 analyzed spots.
KP-25	99.6±1.8	Granodiorite	28°57'23.83"S-70°53'02.45"W (6795313N-316395E)-H 812 m	Cachiyuyo Batholith west of Tricolor; weighted mean of 26 analyzed spots.
KP-20	99.1±1.9	Diorite	29°07'10.20"S-70°57'10.82"W (6777152N-309969E)-H 1288 m	Cachiyuyo Batholith at Pajonales; weighted mean of 25 of 26 analyzed spots; excluded one spot at 106.7 Ma.

MS technique following procedures described by Gehrels *et al*. (2008) and Maksaev *et al*. (2009), who provided a detailed discussion of the sample-preparation techniques, analytical methods, and data analysis. The reported ages are based on $^{206}Pb/^{238}U$ ratios because they are better constrained for young rocks than the $^{207}Pb/^{235}U$ and $^{206}Pb/^{207}Pb$ ratios, which present significantly higher errors; all reported final ages and weighted mean ages have uncertainties at the two-sigma level.

4.1.2. $^{40}Ar/^{39}Ar$ dating

7 mica samples (biotite, muscovite, sericite) from the altered Dos Amigos and Tricolor porphyries and 2 biotite samples from the Cachiyuyo Batholith were dated by the step-heating $^{40}Ar/^{39}Ar$ method. The $^{40}Ar/^{39}Ar$ ages are summarized in Table 2 and the analytical data are included in appendix B. The analytical work was performed at the Stanford University using the step-heating technique following procedures of Marsh *et al*. (1997), who provided a detailed discussion of the sample-preparation techniques, analytical methods, and data analysis. Plateaus were defined using the criteria of Dalrymple and Lamphere (1971) and Fleck *et al*. (1977), specifying the presence of at least three contiguous gas fractions that together represent more than 50 percent of the total ^{39}Ar released from the sample and with apparent ages within error of each other. All $^{40}Ar/^{39}Ar$ plateau ages and weighted mean $^{40}Ar/^{39}Ar$ ages are reported with errors at the two-sigma level; besides, in order to avoid under-estimate analytical uncertainties, the errors have further been enhanced multiplying by $(MSWD)^{1/2}$ for those weighted mean ages with a mean square of weighted deviates higher than 2.

4.1.3. Fission-track and (U-Th)/He dating

Apatite from one sample of the Dos Amigos porphyry (KP-14) was dated by fission-track chronology at the laboratory of Apatite and Zircon Inc. (Viola, Idaho, USA) using laser ablation ICP-MS to estimate the uranium concentrations of the apatite grains for which spontaneous fission tracks were counted (*e.g*., Hasebe *et al*., 2004; Donelick *et al*., 2005); a summary of analytical data are included in appendix C. The analysis included the measurement of the maximum fission-track etch-pit diameters oriented within 5° of the c axis of the apatite crystal (Dpar) in order to consider fission-track annealing variability among different apatite species in thermal history modeling (Carlson *et al*., 1999). Irradiation of the apatite sample with ^{252}Cf was used to increase the amount of etched confined track for length measurement. The AFTSolve multi-kinetic inverse modelling program of apatite fission track data (Ketcham *et al*., 2000) was used to derive time-temperature history for the Dos Amigos porphyry from the apatite fission-track data. This program

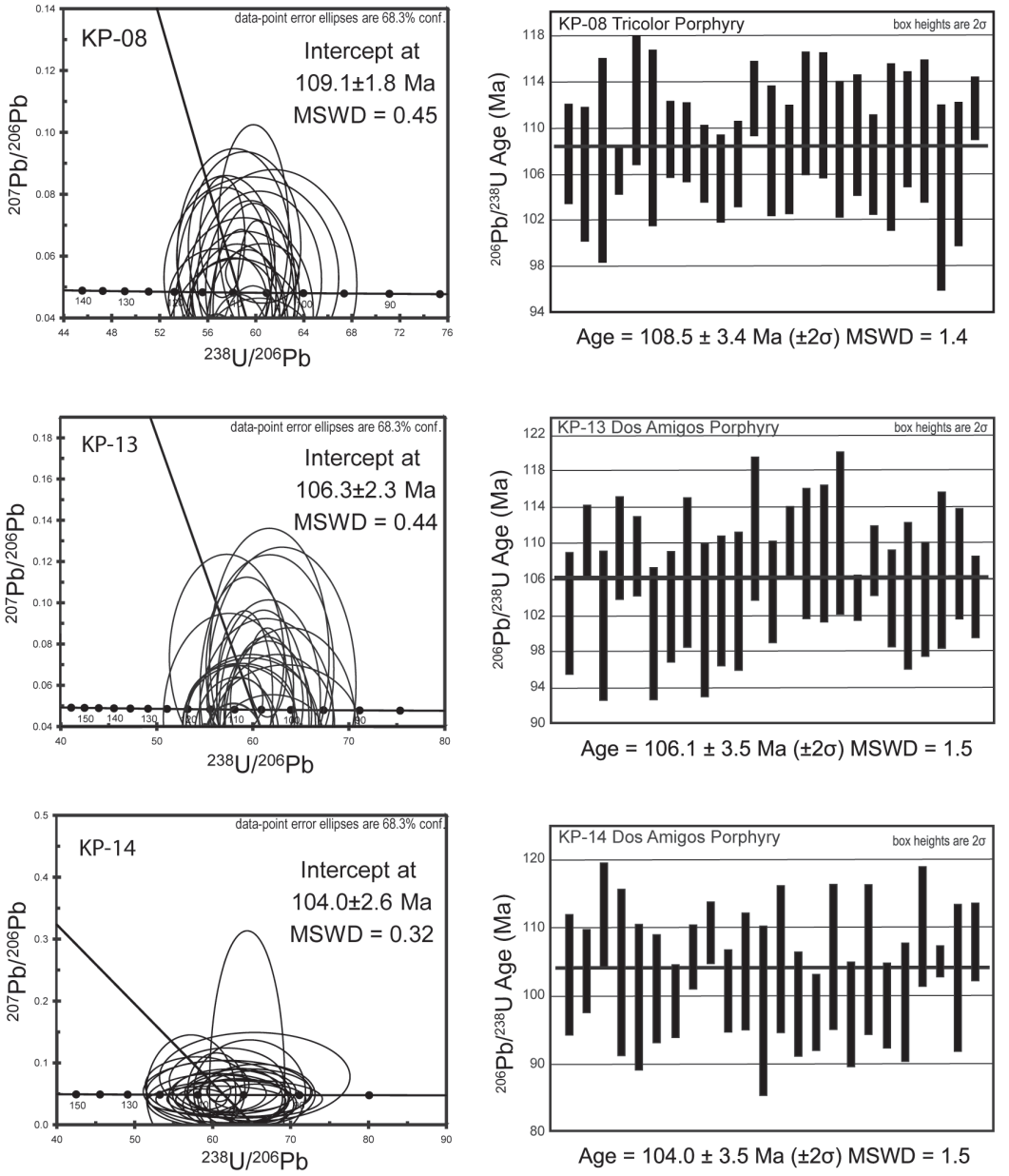

FIG. 7. Plot of U-Pb zircon ages for individual LA-ICP-MS analyses from samples KP-08, KP-13 and KP-14 from mineralized Tricolor and Dos Amigos porphyries. The thick line shows the respective weighted average age (error bars are at ±2σ). As a reference, Tera-Wasserburg plots of the U-Pb data with ellipses at ±1σ are shown.

implements various laboratory calibrations of the behavior of fission tracks in apatite in response to heating and cooling histories, and calculates the range of thermal histories that are potentially consistent with the measured age and the measured frequency distribution of confined track lengths. Full details concerning these calibrations and the various uses of AFTsolve are given in Carlson *et al*. (1999), Donelick *et al*. (1999), Ketcham *et al*. (1999, 2000). 20,000 random time-temperature paths are created by a Monte Carlo scheme, and for each path the resulting fission-track age and track length

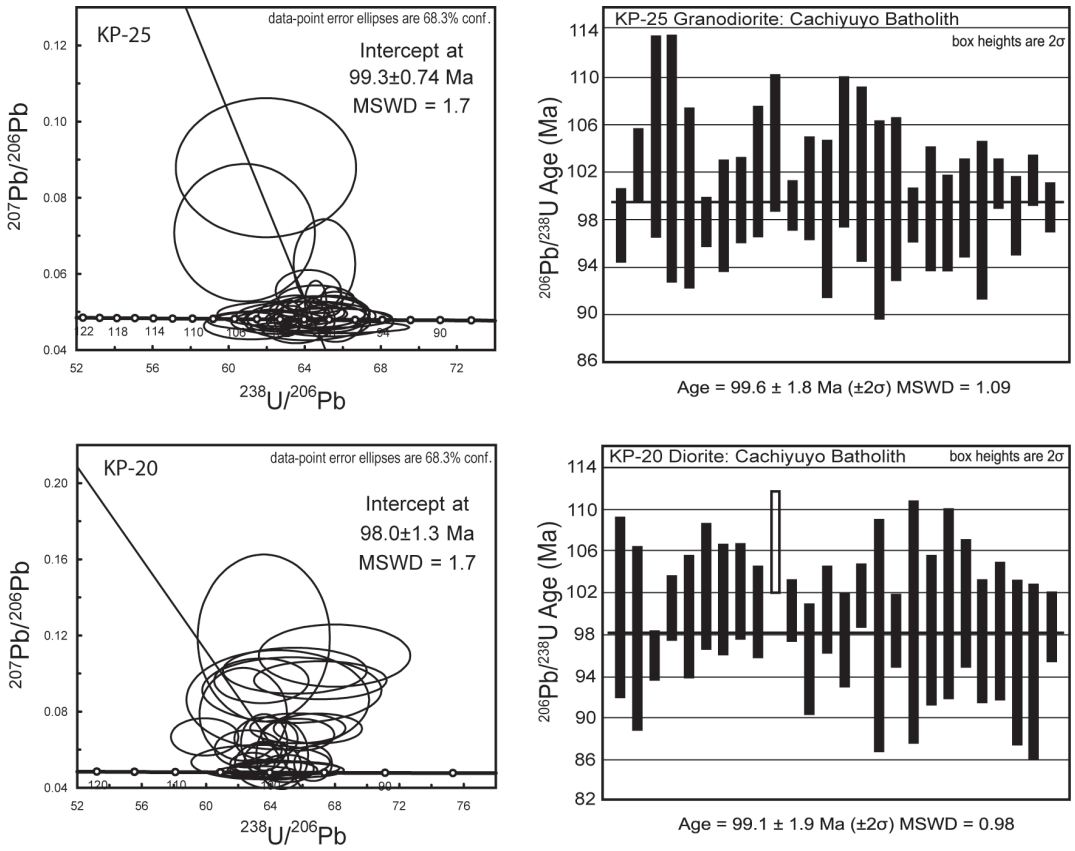

FIG. 8. Plot of U-Pb zircon ages for individual LA-ICP-MS analyses from samples KP-25 and KP-20 from the unaltered Cachiyuyo Batholith. The thick line shows the respective weighted average age (the unshaded bar was excluded from age calculation; error bars are at ±2σ). As a reference, Tera-Wasserburg plots of the U-Pb data with ellipses at ±1σ are shown.

distribution are calculated, and the goodness-of-fit between calculated and measured data is evaluated by a Kolmogorov-Smirnov test. The program maps out the time-temperature regions that envelop all thermal histories with 'good' and 'acceptable' fit, corresponding to goodness-of-fit values from 0.5 to 1 and from 0.05 to 0.5, respectively.

Apatite from the same sample (KP-14) from the Dos Amigos porphyry was also dated by the (U-Th)/He method at Stanford University by argon laser heating for He extraction and at UC Santa Cruz by sector ICP-MS for U-Th determinations; an analytical uncertainty of 7 percent is estimated for the apatite analyses; the analytical data are included in appendix C. Replicate analyses yielded concordant ages and the final (U-Th)/He ages reported include an alpha-ejection correction that accounts for diffusion-domain-dependent loss of the daughter nuclide (after Farley *et al*., 1996 and Farley, 2002).

4.2. Results

4.2.1. U-Pb dating

Two samples from the potassic-altered, mineralized porphyry, collected at the bottom of the open pit in the Dos Amigos mine (KP-13, KP-14; Fig. 5), yielded U-Pb ages of 106.1±3.5 and 104.0±3.5 Ma, respectively. In addition, a sample from the Tricolor porphyry (KP-08) also potassic-altered yielded a U-Pb age of 108.5±3.4 Ma (Figs. 5 and 7). These ages are indistinguishable from each other, as they overlap within analytical error; they correspond to the Albian according to the International Stratigraphic Chart, 2008.

TABLE 2. SUMMARY OF $^{40}Ar/^{39}Ar$ STEP-HEATING AGES.

a. $^{40}Ar/^{39}Ar$ step-heating ages that defined a plateau (>50% of released gas).

Sample	Location (geodetic) and UTM (datum: PSAD56)	Material dated	Plateau age, Ma±2σ	MSWD	Isochron age, Ma±2σ	MSWD	Comments
KP-10	28°57'18.72"S-70°52'41.86"W (6795479N-316950E)-H 837 m	Muscovite	96.3±3.7	0.54	97.8±1.2	1.5	Altered porphyry at Tricolor
KP-16	28°59'12.59"S-70°52'36.01"W (6791976N-317164E)-H 852 m	Sericite	96.1±1.0	0.05	96.2±0.5	0.41	Altered porphyry at Dos Amigos
KP-20	29°07'10.20"S-70°57'10.82"W (6777152N-309969E)-H 1288 m	Biotite	94.8±0.9	0.95	94.5±0.8	24	Unaltered Cachiyuyo Batholith at Pajonales
KP-26	28°58'40.63"S-70°52'38.47"W (6792959N-317164E)-H 880 m	Sericite	85.8±1.2	2.0	88.6±9.0	22	Underground sample of sericitized fragments of the Marisol hydrothermal breccia with tourmaline matrix

b. $^{40}Ar/^{39}Ar$ step-heating ages with irregular age spectra (MSWD>2).

Sample	Location UTM (Datum: PSAD56)	Material dated	Weighted mean age*, Ma±2σ x $(MSWD)^{1/2}$	MSWD	Comments
KP-09	28°57'19.65"S-70°52'42.62"W (6795450N-316930E)-H 840 m	Biotite	105.4±4.9	2.2	Foliated porphyry at Tricolor
KP-12	28°57'17.12"S-70°52'38.03"W (6795530N-317053E)-H 846 m	Biotite	104.1±5.1	7.3	Biotitized rock at Tricolor (potassic alteration) ; spectrum with age gradient from 95 to 105 Ma
KP-10	28°57'18.72"S-70°52'41.86"W (6795479N-316950E)-H 837 m	Biotite	97.1±2.5	8.0	Altered porphyry at Tricolor; spectrum with age gradient from 95 to 99 Ma
KP-25	28°57'23.83"S-70°53'02.45"W (6795313N-316395E)-H 812 m	Biotite	96.9±3.9	16	Unaltered Cachiyuyo Batholith immediately west of Tricolor
KP-13	28°59'10.62"S-70°52'47.06"W (6792032N-316864E)-H 730 m	Biotite	96.9±1.4	4.0	Altered porphyry from the Dos Amigos mine pit

- The error of these ages has been enhanced multiplying by $(MSWD)^{1/2}$ due to the dispersion of apparent ages of the selected steps.

A sample of granodiorite from the Cachiyuyo Batholith immediately west of Tricolor (KP-25) yielded a U-Pb age of 99.6±1.8 Ma (Fig. 5) and a diorite sample from the same batholith, but collected 19 km to the southwest (KP-20) yielded an indistinguishable U-Pb age of 99.1±1.9 Ma (Fig. 8).

4.2.2. $^{40}Ar/^{39}Ar$ dating

Most of the age spectra obtained are irregular implying disturbance of the K-Ar isotopic system of the dated micas (Figs. 9 and 10). Only four age spectra define plateaus with at least 50 percent of the released argon and with apparent ages within error of each other (Table 2a). The samples from the

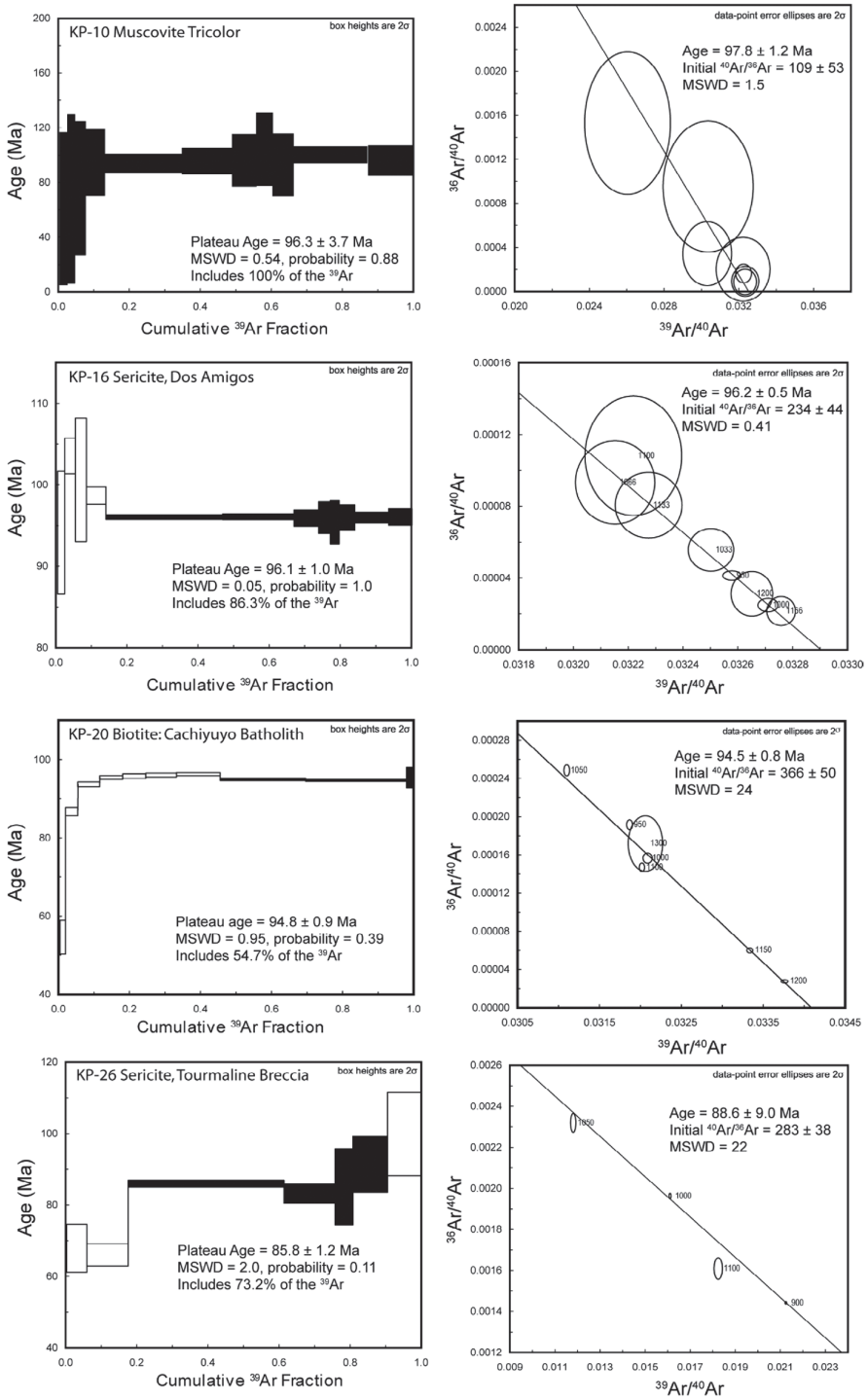

FIG. 9. Apparent $^{40}Ar/^{39}Ar$ age spectra and inverse isochrons for samples that defined plateaus from the Domeyko alteration zone and the Cachiyuyo Batholith. The black boxes indicate the steps used to derive the respective plateau $^{40}Ar/^{39}Ar$ ages.

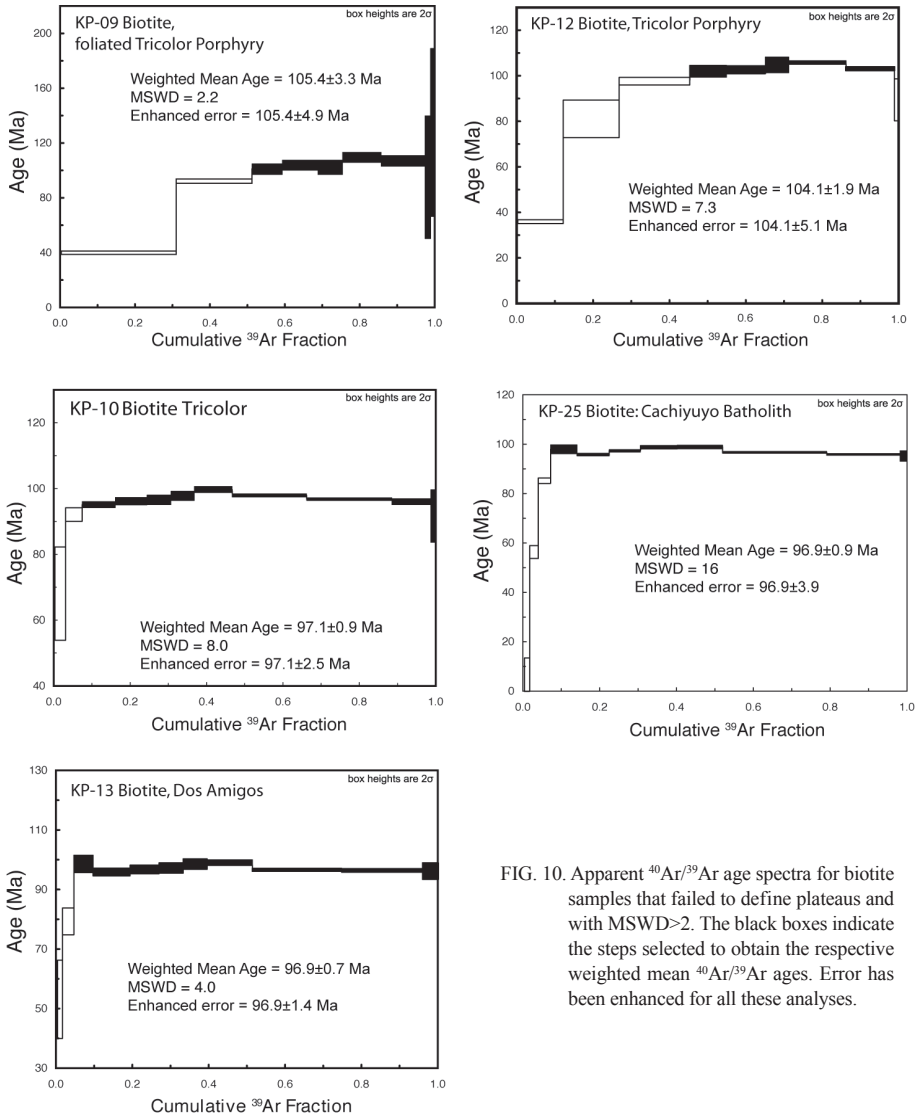

FIG. 10. Apparent $^{40}Ar/^{39}Ar$ age spectra for biotite samples that failed to define plateaus and with MSWD>2. The black boxes indicate the steps selected to obtain the respective weighted mean $^{40}Ar/^{39}Ar$ ages. Error has been enhanced for all these analyses.

Domeyko alteration zone yielded $^{40}Ar/^{39}Ar$ plateau ages for sericite and muscovite from 96.3±3.7 to 85.8±1.2 Ma, and a $^{40}Ar/^{39}Ar$ plateau age of 94.8±0.9 Ma was obtained for biotite from the Cachiyuyo batholith (Table 2a; Fig. 9). Yet, the $^{40}Ar/^{39}Ar$ plateau ages of 96.3±3.7 and 96.1±1.0 Ma for muscovite and sericite from the altered porphyry stocks (KP-10, KP-16; Table 2a) are much younger than their respective U-Pb ages of 108.5±3.4 and 106.1±3.5 Ma, and the $^{40}Ar/^{39}Ar$ plateau age of 94.8±0.9 Ma obtained for biotite from the batholith (KP-20) is also younger than its U-Pb age of 99.1±1.9 Ma. Thus, these $^{40}Ar/^{39}Ar$ plateaus represent minimum cooling ages; in fact, some of the spectra (KP-10, KP-16) have relatively large errors of the apparent ages of individual steps and their respective inverse isochrons show initial $^{40}Ar/^{36}Ar$ ratios lower than the 295.5 value of atmospheric argon, which is consistent with argon loss (Fig. 9). The youngest $^{40}Ar/^{39}Ar$ plateau age of 85.8±1.2 Ma for sericite from the Marisol tourmaline breccia probably reflect argon loss as well.

The remaining five biotite samples show significant disparity in their apparent ages of individual

degassing steps, even for selected portions of the respective age spectra (MSWD>2; Fig. 10). Therefore, their analytical uncertainty has been enhanced yielding weighted mean $^{40}Ar/^{39}Ar$ ages from 105.4±4.9 to 96.9±1.4 Ma (Table 2b). Despite of disturbance and imprecision these ages for biotite overlap within error with the U-Pb dates that were obtained for the Domeyko alteration zone and the Cachiyuyo Batholith (Fig. 11).

4.2.3. Fission-track and (U-Th)/He thermochronology

Sample KP-14 from the Dos Amigos porphyry yielded a LA-ICP-MS apatite fission-track age of 59.8±9.8 Ma (±2σ). The apatite track length distribution is unimodal, relatively narrow and negatively skewed (Skewness=-1.66) with a mean track length of 13.66±0.17 µm and a standard deviation of 1.98 µm (Fig. 12). Its Dpar is 1.58 µm.

Duplicate (U-Th)/He ages of 44.7±3.7 and 44.0±4.2 Ma were obtained on the same apatite sample from the Dos Amigos porphyry (KP-14), attesting to analytical reproducibility.

4.3. Discussion

The U-Pb zircon ages are interpreted as crystallization ages for the intrusions considering that zircon has the highest known closure temperature for Pb diffusion, which exceeds 900ºC for zircons of typical sizes (Cherniak and Watson, 2000 and references therein). Thus two thermal events have occurred related to the emplacement of intrusive bodies; the Dos Amigos and Tricolor porphyry stocks of the Domeyko alteration zone crystallized during the Albian (between 108.5±3.4 and 104.0±3.5 Ma), and the neighboring, unaltered Cachiyuyo Batholith crystallized later, during the Cenomanian between 99.6±1.8 and 99.1±1.9 Ma, thereby confirming geological relationships.

The $^{40}Ar/^{39}Ar$ data for hydrothermal micas indicate a minimum Late Cretaceous age for hydrother-

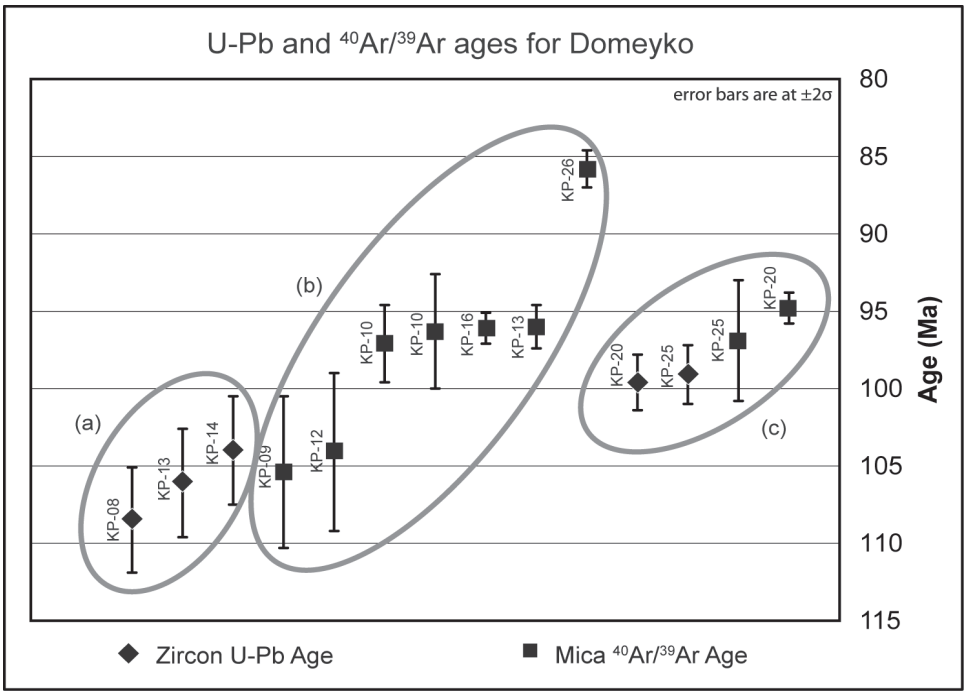

FIG. 11. Summary graph of the geochronological data for the Domeyko Alteration Zone and the neighboring Cachiyuyo Batholith, with sample identification labels: **a.** crystallization U-Pb zircon ages for the Dos Amigos and Tricolor porphyries; **b.** $^{40}Ar/^{39}Ar$ ages for micas from the Domeyko alteration zone; note that despite disturbance, reflected by large error bars, most ages coincide within error with U-Pb ages for the batholith; **c.** crystallization U-Pb and $^{40}Ar/^{39}Ar$ cooling ages for the unaltered Cachiyuyo Batholith.

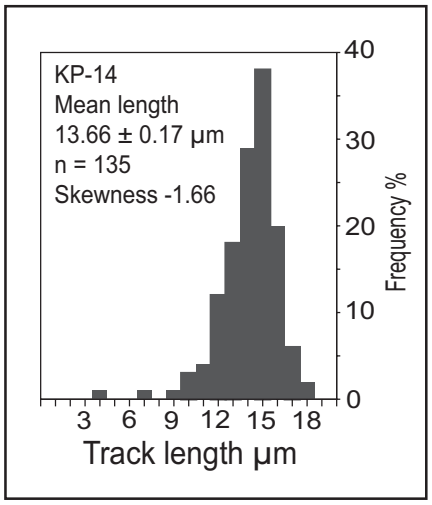

FIG. 12. Histogram showing the distribution of track lengths of apatite sample KP-14 from the Dos Amigos porphyry. The negatively skewed, unimodal distribution of track lengths is compatible with a simple monotonic cooling of the apatite through the temperature range of the apatite partial annealing zone (~125-60°C).

mal activity in the Domeyko alteration zone, but the disparity and/or imprecision of the $^{40}Ar/^{39}Ar$ ages precludes a more accurate age determination. These micas may have been formed during cooling of the porphyry stocks and/or later, during the cooling stage of the neighboring Cachiyuyo Batholith (Fig. 11). Nevertheless, despite disturbance, most $^{40}Ar/^{39}Ar$ ages for alteration micas coincide within error limits of the U-Pb ages, especially those obtained for the batholith (Fig. 11), indicating that these $^{40}Ar/^{39}Ar$ ages record cooling of the Cachiyuyo Batholith. Thus, the thermal event related to the emplacement of the Cachiyuyo Batholith is inferred to have partially or completely reset the isotopic clock of the hydrothermal alteration micas in the adjacent Domeyko Alteration zone.

The crystallization ages obtained for the Dos Amigos porphyry of the Domeyko alteration zone are comparable with the whole rock K-Ar age of 104±3 Ma reported by Reyes (1991) for sericitized porphyry of the Andacollo copper-gold porphyry deposit and with a U-Pb zircon age of 104.0±3.3 Ma for the altered Culebrón porphyry stock located in the center of the Andacollo deposit (our unpublished data). These ages confirm that both deposits are part of the same regional mid-Cretaceous porphyry copper mineralization episode.

The apatite fission-track age of 59.8±9.8 Ma (±2σ) for the Dos Amigos porphyry is significantly younger than the U-Pb and $^{40}Ar/^{39}Ar$ ages of 104.0±3.5 Ma and 96.0±1.4 Ma obtained for this mineralized intrusion, respectively. In addition, the track length distribution (Fig. 12) is comparable to the typical track length distribution of 'undisturbed basement' (Gleadow *et al*., 1986; Green *et al*., 1989), which normally results from a progressive monotonic cooling through the temperature range of the apatite partial annealing zone (~125-60°C; Laslett *et al*., 1987; Reiners *et al*., 2005). It is apparent that cooling through the ~125-60°C temperature range occurred considerably later than the igneous and hydrothermal thermal events detected in the Domeyko alteration zone, which is consistent with the apatite fission-track age record of exhumation-cooling. Assuming a present-day temperature of 15°C, a model time-temperature path was generated from the fission-track data of the FT-14 apatite sample using the AFTSolve multi-kinetic inverse modeling software (Ketcham *et al*., 2000). According to this model the apatite sample started to accumulate tracks at 62.6±10.2 Ma and progressively cooled with time through the temperature range of the apatite partial annealing zone (APAZ: ~125° to 60°C) during the Paleocene (Fig. 13). Therefore it is inferred that the Dos Amigos porphyry cooled through the ~125-60°C temperature range during the Paleocene in response to exhumation.

The apatite (U-Th)/He age of 44.7±3.7 Ma provides further support to the above interpretation considering the even lower temperature range of the apatite He partial retention zone (~85-40°C; Wolf *et al*., 1998; Shuster *et al*., 2006). The apatite cooled through the ~85-40°C temperature range during the Eocene, which is coherent with the modeled cooling path from the apatite fission-track data for the Dos Amigos porphyry (Fig. 13). Thus the combined fission-track and (U-Th)/He thermochronological data indicate that the Dos Amigos porphyry was exhumed during the Paleocene-Eocene period. The exhumation during this time probably was an effect of denudation, which in turn could be consequence of surface uplift and erosion, resulting from major tectonic compressive events in northern Chile, such as the 'K-T' tectonic event near the Cretaceous-Tertiary boundary in the region (Cornejo *et al*., 2003; Charrier *et al*., 2007) and the important Eocene Incaic compressive tectonism that affected

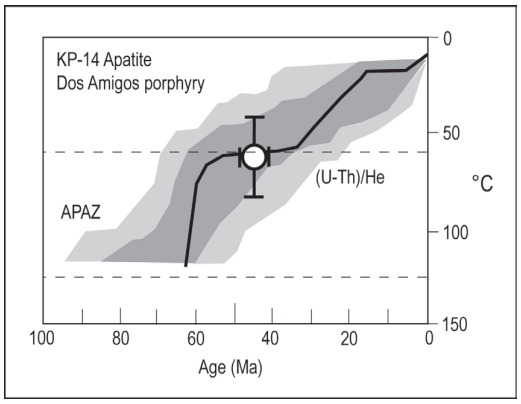

FIG. 13. Time-temperature model of the low temperature cooling history using the fission track data of the apatite sample KP-14 from the Dos Amigos porphyry (AFTSolve best fit line and dark and light gray shading of good and acceptable fit solutions are shown; see text for discussion). The temperature range of the apatite partial annealing zone (APAZ) is indicated by dashed lines. As a reference, the (U-Th)/He age obtained for the same sample is inserted with ±2σ error bars; its vertical bars show the temperature range of the apatite He retention zone.

northern Chile and Peru (Charrier and Vicente, 1972; Maksaev, 1978, 1979).

The exhumation cooling of the Dos Amigos porphyry stock through the apatite He partial retention zone (~85-40°C; Wolf *et al*., 1998) at 44.7±3.7 Ma additionally signifies that a maximum of some 2 km of rock cover may have been removed during the last 44 Myr, accepting a geothermal gradient of 30°C/km. Although the actual paleogeothermal gradient is uncertain, this implies a very low mean exhumation rate since the mid-Eocene (<0.05 mm/yr). Furthermore, the apatite (U-Th)/He age of 44.7±3.7 Ma also provides a maximum age for the formation of the supergene enrichment blanket at Dos Amigos, because the porphyry had to be exhumed to expose sulfides to the effects of oxidative weathering and chalcocite precipitation within the zone of cool groundwater at the time.

The chalcocite blanket at Dos Amigos, located between 740 and 800 m elevation probably developed beneath a low hill within the Miocene Atacama pediplain at roughly the same time as the enrichment at Andacollo (*e.g*., Sillitoe, 2005), considering that terrace relics of the Miocene Atacama Gravels partly surround the Domeyko alteration zone and slope gently westwards from 950 m to 780 m above sea level.

5. Conclusions

The tonalitic to granodioritic porphyry stocks of Dos Amigos and Tricolor in the Domeyko alteration zone crystallized during the Albian (U-Pb ages from 108.5±3.4 to 104.0±3.5 Ma). Hydrothermal alteration of the types: potassic, sericitic, kaolinite-illite and propylitic are zoned around these stocks, and stockwork copper mineralization is fundamentally restricted to these porphyries. Therefore the data confirm that these porphyry copper centers are part of the regional, mid-Cretaceous porphyry copper mineralization episode recognized along the eastern part of the Coastal Cordillera of northern Chile, and with identical U-Pb ages as the Culebrón porphyry of the Andacollo copper-gold deposit.

The Cachiyuyo Batholith that marks the western border of the Domeyko alteration zone crystallized later during the Cenomanian (U-Pb ages 99.1±1.9 and 99.6±1.8 Ma). Most of $^{40}Ar/^{39}Ar$ ages obtained for hydrothermal biotite and sericite from the Tricolor and Dos Amigos porphyry centers overlap with the U-Pb ages obtained for the batholith. They establish a minimum Late Cretaceous age for hydrothermal activity, even though it is inferred that they reflect the effect of the thermal overprint imposed by post-mineralization batholith emplacement.

The apatite fission-track and (U-Th)/He thermochronological data are compatible with exhumation-cooling of the Dos Amigos porphyry during the Paleocene-Eocene, probably related to denudation resulting from uplift imposed by the K-T and Incaic compressive tectonism. Furthermore, the apatite (U-Th)/He age of 44.7±3.7 Ma provides a maximum age for the supergene enrichment processes that formed the chalcocite blanket of this porphyry system, but also implies a very low mean exhumation rate of the porphyry since the late Eocene.

Acknowledgments

Conicyt, Chile, through Fondecyt Grant 1040492 to V. Maksaev and F. Munizaga, provided financial support for this study. The investigation of the Domeyko zone was part of the M.Sc. Thesis of A. Almonacid. The CEMIN mining company granted access to the Dos Amigos mine; we are particularly thankful to D. Ibaceta, Mine Manager; Mr. L. Castro, Mine Administrator, and to Mr. A. Álvarez, Mine Supervisor. Reviews by J. Perelló, R.J. Pankhurst,

and R.H. Sillitoe contributed to improve this paper; a previous version also benefited from evaluations by K. Hickey and an anonymous reviewer.

References

Almonacid, A. 2007. Geología de la zona de alteración de Domeyko y del yacimiento de cobre Dos Amigos, Región de Atacama, Chile. M.Sc. Thesis (Unpublished), Universidad de Chile, Departamento de Geología: p 114.

Arabasz, W.J. 1971. Geological and geophysical studies of the Atacama Fault Zone in Northern Chile. Ph.D. Thesis (Unpublished), Californian Institute of Technology: 264 p. Pasadena, California, U.S.A.

Arévalo, C. 2005a. Carta Copiapó, Región de Atacama. Servicio Nacional de Geología y Minería, Carta Geológica de Chile, Serie Geología Básica 91: 54 p., escala 1:100.000.

Arévalo, C. 2005b. Carta Los Loros, Región de Atacama. Servicio Nacional de Geología y Minería, Carta Geológica de Chile, Serie Geología Básica 92: 54 p., escala 1:100.000.

Arévalo, C.; Mourgues, F.A.; Jaillard, E.; Bulot, L.G. 2005. Comparative evolution of the Lower Cretaceous Pluto-volcanic arc and back-arc from the Atacama Region, Chile. *In* International Symposium on Andean Geodynamics (ISAG), No. 6, Extended Abstracts: 57-60. Barcelona.

Arévalo, C.; Grocott, J.; Martin, W.; Pringle, M.; Taylor, G. 2006. Structural setting of the Candelaria Fe oxide Cu-Au deposit, Chilean Andes (27°30'S). Economic Geology 101: 819-841.

Boric, R.; Díaz, F.; Maksaev, V. 1990. Geología y yacimientos metalíferos de la Región de Antofagasta, Servicio Nacional de Geología y Minería, Boletín 40: p 246.

Bourgois, J.; Toussaint, J.F.; González, H.; Azema, J.; Calle, B.; Desmet, A.; Murcia, L.; Acevedo, A.; Parra, E.; Tournon, J. 1987. Geological history of the Cretaceous ophiolitic complexes in northwestern South America (Colombian Andes). Tectonophysics 143: 307-327.

Brown, M.; Díaz, F.; Grocott, J. 1993. Displacement history of the Atacama fault system 25°00'S-27°00'S, northern Chile. Geological Society of America Bulletin 105: 1165-1174.

Camus, F. 2002. The Andean porphyry systems. *In* Giant Ore Deposits: Characterisitics, genesis and exploration. (Cooke, D.R.; Pongratz, J.; editors). CODES, Special Publication 4: 5-21. Tasmania, Australia.

Camus, F. 2003. Geología de los sistemas porfíricos en los Andes de Chile. Servicio Nacional de Geología y Minería: 267 p. Chile.

Carlson, W.D.; Donelick, R.A.; Ketcham, R.A. 1999. Variability of apatite fission-track annealing kinetics: I Experimental results. American Mineralogist 34: 1213-1223.

Charrier, R.; Vicente, J.-C. 1972. Liminary and geosyncline Andes: major orogenic phases and synchronical evolutions of the central and Magellan sectors of the Argentine Chilean Andes. Solid Earth Problems Conference, Upper Mantle Project 2: 451-70. Buenos Aires.

Charrier, R.; Pinto, L.; Rodríguez, M.P. 2007. Tectonostatigraphic evolution of the Andean Orogen in Chile. *In* The Geology of Chile (Moreno, T.; Gibbons, W.; editors). The Geological Society: 21-114. London.

Cherniak, D.J.; Watson, E.B. 2000. Pb diffusion in zircon. Chemical Geology 172: 5-24.

Cornejo, P.; Matthews, S.; Pérez, C. 2003. The 'K-T' compressive deformation event in northern Chile (24º-27ºS). Proceeedings. *In* Congreso Geológico Chileno, No. 10, Actas, CD-ROM. Concepción.

Dallmeyer, R.D.; Brown, M.; Grocott, J.; Taylor, G.K.; Treolar, P.J. 1996. Mesozoic magmatic and tectonic events within the Andean plate boundary zone, 26°-27°30'S, North Chile: constraints from $^{40}Ar/^{39}Ar$ mineral ages. The Journal of Geology 104: 19-40.

Dalrymple, G.B.; Lanphere, M.A. 1971. $^{40}Ar/^{39}Ar$ technique of K-Ar dating: A comparison with the conventional technique. Earth and Planetary Science Letters, 12: 300-308.

Dalziel, I.W.D. 1986. Collision and Cordilleran orogenesis: An Andean perspective. *In* Collisional on Tectonics (Coward, M.P.; Ries, A.C.; editors). Geological Society of London Special Publication 19: 389-404. London.

Díaz, A.; Vivallo, W.; Jorquera, R.; Pizarro, N. 2003. Depósitos de Fe, óxidos de Fe-Cu-Au y su relación con el magmatismo del Cretácico Inferior, III Región de Atacama, Chile. *In* Congreso Geológico Chileno, No. 10, Actas, CD-ROM. Concepción.

Donelick, R.A.; Ketcham, R.A.; Carlson, W.D. 1999. Variability of apatite fission track annealing kinetics II: Crystallographic orientation effects. American Mineralogist 84: 301-307.

Donelick, R.A.; O'Sullivan, P.B.; Ketcham, R.A. 2005. Apatite fission track analysis. *In* Low Temperature Thermochronology: Techniques, Interpretations, and Applications (Reiners, P.W.; Ehlers, T.A.; edi-

tors). Reviews in Mineralogy and Geochemistry 58: 49-94.

Espinoza, S. 1990. The Atacama-Coquimbo Ferriferous Belt, Northern Chile. *In* Stratabound Ore Deposits in the Andes (Fontboté, L.; Amstutz, G.C.; Cardozo, M.; Cedillo, E.; Frutos, J.; editors). Springer-Verlag: 353-364. Berlin.

Farley, K.A.; Wolf, R.A.; Silver, L.T. 1996. The effects of long alpha-stopping distances on (U-Th)/He ages. Geochimica et Cosmochimica Acta 60: 4223-4229.

Farley, K.A. 2002. (U-Th)/He dating: Techniques, calibrations, and applications. Reviews in Mineralogy and Geochemistry 47: 819-844.

Fleck, R.J.; Sutter, J.F.; Elliot, D.H. 1977. Interpretation of discordant $^{40}Ar/^{39}Ar$ spectra of Mesozoic tholeiites from Abtarctica. Geochimica et Cosmochimica Acta 41: 15-32.

Gehrels, G.E.; Valencia, V.A.; Ruiz, J. 2008. Enhanced precision, accuracy, efficiency, and spatial resolution of U-Pb ages by laser ablation-multicollector-inductively coupled plasma-mass spectrometry. Geochemistry, Geophysics, and Geosystems 9: Q03017, doi:10.1029/2007GC001805

Gelcich, S.H.; Davis, D.W.; Spooner, E.T.C. 2003. New U-Pb ages for host rocks, mineralization and alteration of iron oxide (Cu-Au) deposits in the Coastal Cordillera of northern Chile. *In* South American Symposium on Isotope Geology, No. 4: 63-66. Salvador de Bahia, Brazil.

Gelcich, S.; Davis, D.W.; Spooner, E.T.C. 2005. Testing the apatite-magnetite geochronometer: U-Pb and $^{40}Ar/^{39}Ar$ geochronology of plutonic rocks, massive magnetite-apatite tabular bodies, and IOCG mineralization in Northern Chile. Geochimica et Cosmochimica Acta 69 (13): 3367-3384.

Gleadow, A.J.W.; Duddy, I.R.; Green, P.F.; Lovering, J.F. 1986. Confined fission track lengths in apatite: a diagnostic tool for thermal history analysis. Contributions to Mineralogy and Petrology 94: 405-415.

Green, P.F.; Duddy, I.R.; Laslett, G.M.; Hegarty, K.A.; Gleadow, A.J.W.; Lovering, J.F. 1989. Thermal annealing techniques of fission tracks in apatite 4 Quantitative modelling techniques and extension to geological timescales. Chemical Geology (Isotope Geoscience Section) 79: 155-182.

Grocott, J.; Taylor, G.K. 2002. Magmatic arc fault systems, deformation partitioning and emplacement of granitic complexes in the Coastal Cordillera, north Chilean Andes (25°30'S to 27°00'S). Journal of the Geological Society of London 159: 425-442.

Hasebe, N.; Barbarand, J.; Jarvis, K.; Carter, A.; Hurford, A.J. 2004. Apatite fission-track chronometry using laser ablation ICP-MS. Chemical Geology 207: 135-145.

Ketcham, R.A.; Donelick, R.A.; Carlson, W.D. 1999. Variability of apatite fission track annealing kinetics III: Extrapolations to geological time scales, American Mineralogist 84: 1235-1255.

Ketcham, R.A.; Donelick, R.A.; Donelick, M.B. 2000. AFTSolve: A program for multi-kinetic modeling of apatite fission-track data. Geological Materials Research 2 (electronic www-based journal of the Mineralogical Society of America).

Laslett, G.M.; Green, P.F.; Duddy, I.R.; Gleadow, A.J.W. 1987. Thermal annealing of fission tracks in apatite 2: A quantitative analysis. Chemical Geology 65: 1-15.

Llaumett, C. 1975. Faja Pacífica de cobres porfíricos y desarrollos de alteración hidrotermal de Chile. *In* Congreso Iberoamericano de Geología Económica, No. 2, Actas 2: 331-348. Buenos Aires.

Llaumett, C.; Olcay, L.; Marín, C.; Marquardt, J.C.; Reyes, E. 1975. El yacimiento de cobre porfídico Andacollo, provincia de Coquimbo, Chile. Revista Geológica de Chile 2: 56-66.

Maksaev, V. 1978. Cuadrángulo Chitigua y sector oriental del Cuadrángulo Cerro Palpana, Región de Antofagasta. Instituto de Investigaciones Geológicas, Carta Geológica de Chile 31: 55 p., escala 1:50.000.

Maksaev, V. 1979. Las Fases Tectónicas Incaica y Quechua en la Cordillera de los Andes del Norte Grande de Chile. *In* Congreso Geológico Chileno, No. 2, Actas 1: B63 B77. Arica.

Maksaev, V.; Munizaga, F.; Fanning, M.; Palacios, C.; Tapia, J. 2006a. SHRIMP U-Pb dating of the Antucoya porphyry copper deposit: new evidence for an Early Cretaceous porphyry-related metallogenic epoch in the Coastal Cordillera of northern Chile. Mineralium Deposita 41 (7): 637-644.

Maksaev, V.; Munizaga, F.; Valencia, V.; Barra, F.; McWilliams, M.; Mathur, R. 2006b. Geochronology of Cretaceous porphyry copper deposits of the Coastal Cordillera of northern Chile (latitudes 26°30' to 30°30'S). Geological Society of America Abstracts with Programs 38 (7): 347.

Maksaev, V.; Townley, B.; Palacios, C.; Camus, F. 2007. Metallic ore deposits. *In* The Geology of Chile (Moreno, T.; Gibbons, W.; editors). The Geological Society, London: 179-199. London.

Maksaev, V.; Munizaga, F.; Valencia, V.; Barra, F. 2009.

LA-ICP-MS zircon U-Pb geochronology to constrain the age of post-Neocomian continental deposits of the Cerrillos Formation, Atacama Region, northern Chile: tectonic and metallogenic implications. Andean Geology 36 (2):264-287.

Marschik, R.; Fonboté, L. 2001. The Candelaria-Punta del Cobre iron oxide Cu-Au (-Zn-Ag) deposits, Chile. Economic Geology 96: 1799-1826.

Marschik, R.; Söllner, F. 2006. Early Cretaceous U-Pb zircon ages for the Copiapó plutonic complex and implications for the IOCG mineralization at Candelaria, Atacama, Region, Chile. Mineralium Deposita 41: 785-801.

Marsh, T.M.; Einaudi, M.T.; McWilliams, M. 1997. $^{40}Ar/^{39}Ar$ geochronology of Cu-Au and Au-Ag mineralization in the Potrerillos district, Chile. Economic Geology 92: 784-806.

Mathur, R.; Marschik, R.; Ruiz, J.; Munizaga, F.; Leveille, R.A.; Martin, W. 2002. Age of mineralization of the Candelaria Fe oxide Cu-Au deposit and the origin of the Chilean Iron Belt, based on Re-Os isotopes. Economic Geology 97: 59-71.

Mortimer, C. 1973. The Cenozoic history of the southern Atacama Desert, Chile. Journal of the Geological Society of London 129: 505-526.

Moscoso, R.; Nasi, C.; Salinas, P. 1982. Geología de la Hoja Vallenar y parte Norte de la Hoja La Serena. Servicio Nacional de Geología y Minería, Carta Geológica de Chile 55: 100 p. Santiago.

Mpodozis, C.; Ramos, V.A. 1990. The Andes of Chile and Argentina. *In* Geology of the Andes and its Relation to Hydrocarbon and Energy Resources (Ericksen, G.E.; Cañas, M.T.; Reinemund, J.A.; editors). Circum-Pacific Council for Energy and Hydrothermal Resources. American Association of Petroleum Geologists, Earth Science Series 11: 59-90. Houston, Texas.

Munizaga, F.; Huete, C.; Hervé, F. 1985. Geocronología K-Ar y razones iniciales $^{87}Sr/^{86}Sr$ de la Franja Pacífica de Desarrollos Hidrotermales. *In* Congreso Geológico Chileno, No. 4, Actas 4: 357-379. Antofagasta.

Nyström, J.O.; Henríquez, F. 1994. Magmatic features of iron ores of the Kiruna type in Chile and Sweden: ore textures and magnetite geochemistry. Economic Geology 89: 820-839.

Oyarzún, R.; Oyarzún, J.; Ménard, J.; Lillo, J. 2003. The Cretaceous Iron Belt of Northen Chile: Role of oceanic plates, a superplume event, and major shear zone. Mineralium Deposita 38: 640-646.

Perelló, J.; Martini, R.; Arcos, R.; Muhr, R. 2003. Buey Muerto: porphyry copper mineralization in the Early Cretaceous arc of northern Chile. *In* Congreso Geológico Chileno, No. 10, Actas, CD-ROM. Concepción.

Reiners, P.W.; Ehlers, T.A.; Zeitler, P.K. 2005. Past, present, and future of thermochronology. *In* Low Temperature Thermochronology: Techniques, Interpretations, and Applications (Reiners, P.W.; Ehlers, T.A.; editors). Reviews in Mineralogy and Geochemistry 58: 1-18.

Reyes, M. 1991. The Andacollo strata-bound gold deposit, Chile, and its position in a porphyry copper-gold system. Economic Geology 86: 1301-1316.

Ruiz, C.; Corvalán, J.; Klohn, C.; Klohn, E.; Levi, B. 1965. Geología y yacimientos metalíferos de Chile. Instituto de Investigaciones Geológicas: 305 p. Santiago.

Scheuber, E.; Andriessen, P.A.M. 1990. The kinematic and geodynamic significance of the Atacama fault zone, northern Chile. Journal of Structural Geology 12: 24-257.

Scheuber, E.; Hammerschmidt, K.; Friedrichsen, H. 1995. $^{40}Ar/^{39}Ar$ and Rb-Sr analyses from ductile shear zones from the Atacama Fault Zone, Northern Chile: the age of deformation. Tectonophysics 250: 61-87.

Scheuber, E.; González, G. 1999. Tectonics of the Jurassic-Early Cretaceous magmatic arc of the north Chilean Coastal Cordillera (22°-26°S): a story of crustal deformation along a convergent plate boundary. Tectonics 18: 895-910.

Segerstrom, K.; Parker, R.L. 1959. Cuadrángulo Cerrillos, Provincia de Atacama. Instituto de Investigaciones Geológicas, Carta Geológica de Chile 2: 33 p., escala 1:50.000.

Shuster, D.L.; Flowers, R.M.; Farley, K.A. 2006. The influence of natural radiation damage on helium diffusion kinetics in apatite. Earth and Planetary Science Letters 249: 148-161.

Sillitoe, R.H. 2003. Iron oxide-copper-gold deposits: an Andean view. Mineralium Deposita 38: 787-812.

Sillitoe, R.H. 2005. Supergene oxidized and enriched porphyry copper and related deposits. *In* Economic Geology One Hundredth Anniversary Volume (Heddenquist, J.W.; Thompson, J.F.H.; Goldfarb, R.J.; Richards, J.P.; editors). Society of Economic Geologists: 723-768. Littleton, Colorado, U.S.A.

Sillitoe, R.H.; Perelló, J. 2005. Andean copper province: tectonomagmatic settings, deposit types, Metallogeny, exploration, and discovery. *In* Economic Geology One Hundredth Anniversary Volume (Hedenquist, J.W.; Thompson, J.F.H.; Goldfarb, R.; Richards, J.; editors). Society of Economic Geologists: 845-890. Littleton, Colorado, USA.

Taylor, G.K.; Grocott, J.; Pope, A.; Randall, D.E. 1998. Mesozoic fault systems, deformation and fault block rotation in the Andean forearc; a crustal scale strike-slip duplex in the Coastal Cordillera of northern Chile. Tectonophysics 299: 93-109.

Ullrich, T.D.; Clark, A.H. 1999. The Candelaria copper-gold deposit, Region III, Chile: Paragenesis, geochronology and fluid composition. *In* Mineral Deposits: Processes to Processing. Balkema: 201-204. Rotterdam.

Vila, T.; Lindsay, N.; Zamora, R. 1996. Geology of the Manto Verde copper deposit, Northern Chile: a specularite-rich, hydrothermal-tectonic breccia related to the Atacama Fault Zone. *In* Andean copper deposits: new discoveries, mineralization styles and metallogeny (Camus, F.; Sillitoe, R.H.; Petersen, R.; editors). Society of Economic Geologists Special Publication 5: 157-170.

Wolf, R.A.; Farley, K.A.; Kass, D.M. 1998. Modeling of the temperature sensitivity of the apatite (U-Th)/He thermochronometer. Chemical Geology 148: 105-114.

Manuscript received: March 12, 2009; revised/accepted: October 16, 2009.

APPENDIX A. ZIRCON LA-ICP-MS U-Pb ANALYTICAL DATA.

Sample	U (ppm)	Th (ppm)	$^{206}Pb/^{204}Pb$ common	U/Th	$^{207}Pb/^{235}U$	±(%)	$^{206}Pb/^{238}U$	±(%)	Err. corr.	$^{207}Pb/^{235}U$ age	±(Ma)	Best Age $^{206}Pb/^{238}U$	±(Ma)
KP08-1	153	138	463	1.1	0.08210	50.16	0.01686	3.81	0.08	80.1	37.9	107.8	4.1
KP08-2	130	79	479	1.7	0.06585	40.69	0.01659	5.21	0.13	64.8	25.2	106.1	5.5
KP08-3	57	30	251	1.9	0.12259	41.35	0.01677	8.06	0.19	117.4	44.8	107.2	8.6
KP08-4	200	148	823	1.3	0.11275	30.05	0.01664	1.76	0.06	108.5	30.5	106.4	1.9
KP08-5	150	91	559	1.6	0.10989	25.33	0.01760	4.78	0.19	105.9	25.2	112.4	5.3
KP08-7	95	61	225	1.6	0.06945	66.76	0.01708	6.78	0.10	68.2	43.1	109.2	7.3
KP08-8	156	95	567	1.6	0.07587	31.58	0.01706	2.76	0.09	74.3	22.4	109.0	3.0
KP08-9	130	84	555	1.6	0.09042	51.55	0.01701	2.92	0.06	87.9	42.5	108.8	3.1
KP08-10	194	188	473	1.0	0.07398	37.80	0.01673	2.88	0.08	72.5	26.1	107.0	3.1
KP08-11	398	293	2455	1.4	0.12390	12.13	0.01652	3.33	0.27	118.6	13.5	105.6	3.5
KP08-12	183	147	870	1.2	0.15798	32.85	0.01672	3.24	0.10	148.9	44.5	106.9	3.4
KP08-13	165	197	465	0.8	0.05314	58.47	0.01762	2.65	0.05	52.6	29.5	112.6	3.0
KP08-14	93	53	246	1.8	0.11004	29.47	0.01690	4.97	0.17	106.0	29.2	108.0	5.3
KP08-15	193	156	189	1.2	0.11454	38.15	0.01678	4.16	0.11	110.1	39.0	107.3	4.4
KP08-16	155	125	724	1.2	0.12967	34.70	0.01741	4.50	0.13	123.8	39.7	111.3	5.0
KP08-17	143	139	722	1.0	0.14322	29.47	0.01739	4.69	0.16	135.9	36.8	111.1	5.2
KP08-18	125	73	441	1.7	0.14785	32.09	0.01693	5.23	0.16	140.0	41.1	108.2	5.6
KP08-19	103	72	513	1.4	0.08811	47.18	0.01711	4.57	0.10	85.7	38.1	109.4	5.0
KP08-20	127	68	514	1.9	0.09741	54.40	0.01671	3.76	0.07	94.4	47.9	106.8	4.0
KP08-21	96	53	372	1.8	0.09740	49.17	0.01695	6.49	0.13	94.4	43.4	108.4	7.0
KP08-22	173	160	503	1.1	0.09902	28.26	0.01720	4.36	0.15	95.9	25.5	109.9	4.8
KP08-23	76	41	476	1.9	0.14263	38.20	0.01718	5.41	0.14	135.4	47.3	109.8	5.9
KP08-24	66	39	300	1.7	0.11418	48.63	0.01627	7.46	0.15	109.8	49.4	104.0	7.7
KP08-25	68	41	215	1.6	0.11917	37.00	0.01658	5.66	0.15	114.3	39.2	106.0	6.0
KP08-26	203	244	1336	0.8	0.15940	19.58	0.01748	2.17	0.11	150.2	27.0	111.7	2.4

KP-08: Tricolor porphyry, weighted mean $^{206}Pb/^{238}U$ age: 108.5±3.4 Ma.

Appendix A. continued.

Sample	U (ppm)	Th (ppm)	$^{206}Pb/^{204}Pb$ common	U/Th	$^{207}Pb/^{235}U$	±(%)	$^{206}Pb/^{238}U$	±(%)	Err. corr.	$^{207}Pb/^{235}U$ age	±(Ma)	Best Age $^{206}Pb/^{238}U$	±(Ma)
KP13-1	49	27	215	1.8	0.09157	53.47	0.01599	6.30	0.12	89.0	44.6	102.3	6.4
KP13-2	194	239	541	0.8	0.08183	32.35	0.01725	3.36	0.10	79.9	24.5	110.2	3.7
KP13-3	43	24	173	1.8	0.08418	53.75	0.01576	7.94	0.15	82.1	41.5	100.8	7.9
KP13-4	78	62	285	1.3	0.08515	51.44	0.01715	4.95	0.10	83.0	40.2	109.6	5.4
KP13-5	131	89	436	1.5	0.08768	46.58	0.01701	3.78	0.08	85.3	37.4	108.7	4.1
KP13-6	48	24	159	2.0	0.09093	71.92	0.01565	6.98	0.10	88.4	59.1	100.1	6.9
KP13-7	77	50	243	1.5	0.08190	33.69	0.01612	5.60	0.17	79.9	25.6	103.1	5.7
KP13-8	62	38	158	1.6	0.09581	53.61	0.01672	7.44	0.14	92.9	46.5	106.9	7.9
KP13-9	46	24	183	1.9	0.13141	73.89	0.01586	8.05	0.11	125.4	83.6	101.4	8.1
KP13-10	37	19	248	1.9	0.16429	56.51	0.01620	6.65	0.12	154.5	77.9	103.6	6.8
KP13-11	36	19	226	1.9	0.15143	54.35	0.01619	7.11	0.13	143.2	70.1	103.5	7.3
KP13-12	48	28	240	1.7	0.17663	45.59	0.01746	6.87	0.15	165.2	67.2	111.6	7.6
KP13-13	59	33	139	1.8	0.09168	90.72	0.01636	5.11	0.06	89.1	74.6	104.6	5.3
KP13-14	120	112	526	1.1	0.12599	21.14	0.01720	3.30	0.16	120.5	23.7	110.0	3.6
KP13-15	110	83	366	1.3	0.11454	30.20	0.01702	6.32	0.21	110.1	31.0	108.8	6.8
KP13-17	83	65	384	1.3	0.09632	46.42	0.01704	6.69	0.14	93.4	40.6	108.9	7.2
KP13-18	55	33	396	1.7	0.10566	76.47	0.01739	7.83	0.10	102.0	71.6	111.1	8.6
KP13-20	168	112	620	1.5	0.14830	21.63	0.01625	2.11	0.10	140.4	28.0	103.9	2.2
KP13-21	108	92	352	1.2	0.13065	47.29	0.01691	3.25	0.07	124.7	54.0	108.1	3.5
KP13-22	65	40	159	1.6	0.10271	51.52	0.01624	4.88	0.09	99.3	47.6	103.9	5.0
KP13-23	91	63	181	1.4	0.10320	67.01	0.01629	7.48	0.11	99.7	61.7	104.1	7.7
KP13-24	60	27	254	2.2	0.11937	59.70	0.01622	5.77	0.10	114.5	62.7	103.7	5.9
KP13-25	38	21	147	1.8	0.09357	53.75	0.01673	7.82	0.15	90.8	45.7	107.0	8.3
KP13-26	51	32	166	1.6	0.13331	63.47	0.01684	5.41	0.09	127.1	73.1	107.7	5.8
KP13-27	98	61	245	1.6	0.11583	41.03	0.01627	4.06	0.10	111.3	42.4	104.1	4.2

KP-13: Dos Amigos porphyry, weighted mean $^{206}Pb/^{238}U$ age: 106.1±3.5 Ma.

Appendix A. continued.

Sample	U (ppm)	Th (ppm)	$^{206}Pb/^{204}Pb$ common	U/Th	$^{207}Pb/^{235}U$	±(%)	$^{206}Pb/^{238}U$	±(%)	Err. corr.	$^{207}Pb/^{235}U$ age	±(Ma)	Best Age $^{206}Pb/^{238}U$	±(Ma)
KP14-1	35	19	116	1.9	0.09831	68.60	0.01612	8.20	0.12	95.2	60.5	103.1	8.4
KP14-2	44	28	165	1.5	0.11308	38.69	0.01619	5.45	0.14	108.8	39.1	103.5	5.6
KP14-3	44	23	174	2.0	0.12151	124.06	0.01748	6.62	0.05	116.4	128.1	111.7	7.3
KP14-4	32	18	157	1.8	0.11975	62.95	0.01617	11.47	0.18	114.8	66.2	103.4	11.8
KP14-5	50	26	119	1.9	0.08938	49.79	0.01560	10.27	0.21	86.9	40.7	99.8	10.2
KP14-6	32	17	131	1.9	0.07174	83.48	0.01580	7.42	0.09	70.4	55.2	101.0	7.4
KP14-7	38	19	131	1.9	0.12924	276.48	0.01552	4.94	0.02	123.4	279.1	99.3	4.9
KP14-8	39	19	181	2.1	0.12921	69.33	0.01654	4.01	0.06	123.4	77.5	105.7	4.2
KP14-9	89	96	264	0.9	0.09617	27.92	0.01708	3.69	0.13	93.2	24.6	109.2	4.0
KP14-10	92	69	377	1.3	0.09363	73.29	0.01574	5.65	0.08	90.9	61.8	100.7	5.6
KP14-11	56	35	144	1.6	0.15936	49.22	0.01619	7.85	0.16	150.1	66.5	103.5	8.1
KP14-12	35	23	149	1.5	0.16344	62.18	0.01529	12.33	0.20	153.7	85.0	97.8	12.0
KP14-13	46	27	189	1.7	0.08875	74.17	0.01648	9.91	0.13	86.3	59.6	105.4	10.3
KP14-14	56	36	191	1.6	0.11425	102.95	0.01545	7.31	0.07	109.8	101.9	98.8	7.2
KP14-15	104	60	143	1.7	0.07183	60.62	0.01525	5.22	0.09	70.4	40.4	97.6	5.0
KP14-16	100	97	274	1.0	0.08943	40.29	0.01653	9.68	0.24	87.0	33.0	105.7	10.1
KP14-17	52	45	130	1.2	0.10293	65.95	0.01520	7.41	0.11	99.5	60.6	97.3	7.1
KP14-18	43	26	132	1.6	0.11572	68.82	0.01646	10.05	0.15	111.2	70.0	105.3	10.5
KP14-19	54	29	116	1.9	0.11596	39.29	0.01540	5.81	0.15	111.4	40.6	98.5	5.7
KP14-20	34	21	89	1.6	0.11058	49.57	0.01548	8.36	0.17	106.5	48.9	99.0	8.2
KP14-21	45	33	145	1.4	0.15082	48.58	0.01724	7.57	0.16	142.6	62.7	110.2	8.3
KP14-22	284	494	1200	0.6	0.12343	20.62	0.01644	1.62	0.08	118.2	22.8	105.1	1.7
KP14-23	42	22	119	1.9	0.09091	49.26	0.01604	10.19	0.21	88.3	40.9	102.6	10.4
KP14-24	60	41	246	1.5	0.11488	45.84	0.01688	4.91	0.11	110.4	46.9	107.9	5.2

KP-14: Dos Amigos porphyry, weighted mean $^{206}Pb/^{238}U$ age: 104.0±3.5 Ma

Appendix A. continued.

Sample	U (ppm)	Th (ppm)	$^{206}Pb/^{204}Pb$ common	U/Th	$^{207}Pb/^{235}U$	±(%)	$^{206}Pb/^{238}U$	±(%)	Err. corr.	$^{207}Pb/^{235}U$ age	±(Ma)	Best Age $^{206}Pb/^{238}U$	±(Ma)
KP20-1	58	5	241	10.7	0.2574	24.7	0.01573	4.3	0.2	232.6	51.5	100.6	4.3
KP20-2	115	230	243	0.5	0.21358	9.1	0.01526	4.5	0.5	196.6	16.2	97.7	4.4
KP20-3	275	212	1045	1.3	0.12202	20.8	0.01545	1.6	0.1	116.9	22.9	98.8	1.6
KP20-4	190	173	1123	1.1	0.1091	11.5	0.01501	1.2	0.1	105.1	11.5	96	1.1
KP20-5	483	439	1186	1.1	0.1385	15.4	0.01572	1.5	0.1	131.7	19	100.6	1.5
KP20-6	696	633	2649	1.1	0.10619	7.4	0.01559	2.9	0.4	102.5	7.2	99.7	2.8
KP20-7	323	215	496	1.5	0.17405	20.6	0.01605	2.9	0.1	162.9	31.1	102.6	2.9
KP20-8	710	546	3275	1.3	0.10588	4.8	0.01584	2.6	0.5	102.2	4.6	101.3	2.6
KP20-9	147	245	238	0.6	0.22197	10.9	0.01471	4.6	0.4	203.5	20.1	94.1	4.3
KP20-10	213	152	683	1.4	0.13308	10.9	0.01597	2.2	0.2	126.9	13	102.1	2.2
KP20-11	319	290	1287	1.1	0.11259	15.7	0.01566	2.1	0.1	108.3	16.1	100.2	2.1
KP20-12	482	344	828	1.4	0.15365	10	0.01669	2.3	0.2	145.1	13.5	106.7	2.4
KP20-13	155	258	255	0.6	0.1983	8	0.0149	4.1	0.5	183.7	13.4	95.4	3.8
KP20-14	481	437	1561	1.1	0.11942	10	0.01568	1.4	0.1	114.5	10.9	100.3	1.4
KP20-15	835	835	3585	1	0.10651	5.8	0.01537	3.3	0.6	102.8	5.7	98.3	3.2
KP20-16	265	530	379	0.5	0.14641	7.8	0.01494	2.7	0.3	138.7	10.1	95.6	2.6
KP20-17	233	166	742	1.4	0.14244	11.4	0.01569	2	0.2	135.2	14.5	100.4	2
KP20-18	279	254	680	1.1	0.14252	8.5	0.01522	2.3	0.3	135.3	10.8	97.4	2.2
KP20-19	459	417	1733	1.1	0.11507	7.6	0.0159	1.5	0.2	110.6	8	101.7	1.5
KP20-20	125	313	227	0.4	0.1927	13.7	0.01531	5.6	0.4	178.9	22.5	97.9	5.5
KP20-21	282	118	1771	2.4	0.10622	9.6	0.01538	1.7	0.2	102.5	9.4	98.4	1.7
KP20-22	334	278	418	1.2	0.18441	20.8	0.01552	5.8	0.3	171.8	32.9	99.2	5.7
KP20-23	521	401	2081	1.3	0.10451	6.6	0.01538	3.6	0.5	100.9	6.3	98.4	3.5
KP20-24	578	578	2383	1	0.1163	12	0.01577	4.5	0.4	111.7	12.7	100.9	4.5
KP20-25	260	650	298	0.4	0.20918	8.6	0.01576	3.1	0.4	192.9	15.1	100.8	3.1
KP20-26	498	383	633	1.3	0.14961	7.9	0.01522	3	0.4	141.6	10.4	97.4	2.9

KP-20: Cachiyuyo Batholith, weighted mean $^{206}Pb/^{238}U$ age: 99.1±1.9 Ma.

Appendix A. continued.

Sample	U (ppm)	Th (ppm)	$^{206}Pb/^{204}Pb$ common	U/Th	$^{207}Pb/^{235}U$	±(%)	$^{206}Pb/^{238}U$	±(%)	Err. corr.	$^{207}Pb/^{235}U$ age	±(Ma)	Best Age $^{206}Pb/^{238}U$	±(Ma)
KP25-1	394	262	2397	1.5	0.1024	9.1	0.01524	1.6	0.2	99	8.5	97.5	1.5
KP25-2	664	349	4737	1.9	0.10647	3.8	0.01604	1.5	0.4	102.7	3.7	102.6	1.5
KP25-3	837	558	752	1.5	0.16051	17.3	0.01644	4	0.2	151.1	24.3	105.1	4.2
KP25-4	572	79	489	7.2	0.19557	14.6	0.01614	5	0.3	181.4	24.3	103.2	5.2
KP25-5	1067	260	7260	4.1	0.10537	6.4	0.01561	3.8	0.6	101.7	6.2	99.8	3.7
KP25-6	992	827	2495	1.2	0.11145	4.8	0.01529	1	0.2	107.3	4.9	97.8	1
KP25-7	468	390	2800	1.2	0.10534	6.3	0.01537	2.3	0.4	101.7	6.1	98.3	2.3
KP25-8	586	391	1876	1.5	0.11919	6.8	0.01558	1.8	0.3	114.3	7.4	99.7	1.8
KP25-9	740	617	5495	1.2	0.10405	5	0.01596	2.7	0.5	100.5	4.8	102.1	2.7
KP25-10	499	384	3401	1.3	0.10441	5.7	0.01634	2.7	0.5	100.8	5.5	104.5	2.8
KP25-11	864	720	5326	1.2	0.10647	2.1	0.01551	1	0.5	102.7	2.1	99.2	1
KP25-12	511	393	3116	1.3	0.10426	8.9	0.01574	2.1	0.2	100.7	8.5	100.6	2.1
KP25-13	885	256	5912	3.3	0.10224	4.8	0.01532	3.4	0.7	98.8	4.6	98	3.3
KP25-14	845	325	6108	2.6	0.10678	4.5	0.01621	3	0.7	103	4.4	103.7	3.1
KP25-15	1111	794	5261	1.4	0.10867	5.7	0.01592	3.6	0.6	104.7	5.7	101.8	3.6
KP25-16	959	1066	4836	0.9	0.09711	4.8	0.01531	4.2	0.9	94.1	4.3	97.9	4.1
KP25-17	675	563	3745	1.2	0.10244	7.8	0.01559	3.4	0.4	99	7.4	99.7	3.4
KP25-18	1094	179	7101	6.1	0.10572	2.9	0.01538	1.1	0.4	102	2.8	98.4	1.1
KP25-19	604	318	4281	1.9	0.10672	6	0.01546	2.6	0.4	103	5.9	98.9	2.6
KP25-20	631	210	3607	3	0.10427	6.7	0.01528	2	0.3	100.7	6.4	97.8	1.9
KP25-21	596	426	3262	1.4	0.11378	5	0.01548	2	0.4	109.4	5.1	99	2
KP25-22	820	745	4246	1.1	0.09995	6.2	0.01531	3.4	0.5	96.7	5.7	97.9	3.3
KP25-23	1362	10517	10517	5.7	0.10937	2.1	0.0158	1	0.5	105.4	2.1	101.1	1
KP25-24	1214	1365	1365	3.5	0.13266	12.5	0.01538	1.6	0.1	126.5	14.9	98.4	1.6
KP25-25	605	4146	4146	1.4	0.10578	6.5	0.01584	1	0.2	102.1	6.3	101.3	1
KP25-28	940	2268	2268	1	0.11238	7.1	0.01549	1	0.1	108.1	7.3	99.1	1

KP-25: Cachiyuyo Batholith; weighted mean $^{206}Pb/^{238}U$ age: 99.6±1.8 Ma.

APPENDIX B. $^{40}Ar/^{39}Ar$ FURNACE STEP HEATING ANALYTICAL DATA.

Temp (°C)	$^{40}Ar^*/^{39}Ar$	±1σ	$^{39}Ar/^{40}Ar$	±1σ	$^{36}Ar/^{40}Ar$	±1σ	^{39}Ar	$^{40}Ar^*$ (%)	K/Ca	Age (Ma)	±1σ (Ma)
KP-10 sericite; J = 0.0018142											
700	18.86766	2.93590	0.01949	0.00053	0.0021400	0.000178	0.000208	36.5	0.5012	60.62	27.83
800	21.06851	3.26045	0.02600	0.00094	0.0015305	0.000264	0.000197	54.6	1.0357	67.56	30.79
850	23.62322	2.58673	0.03033	0.00099	0.0009594	0.000243	0.000268	71.5	2.8434	75.59	24.32
900	29.63530	1.29873	0.03028	0.00054	0.0003472	0.000119	0.000519	89.6	4.1442	94.33	12.08
950	29.44958	0.36127	0.03224	0.00017	0.0001706	0.000035	0.002031	94.8	8.4603	93.75	3.36
1000	30.08253	0.49316	0.03232	0.00025	0.0000940	0.000047	0.001290	97.1	19.2457	95.72	4.58
1025	30.10582	1.02160	0.03326	0.00053	-0.0000041	0.000112	0.000634	100.0	9.8862	95.79	9.50
1050	32.75958	1.42172	0.03380	0.00081	-0.0003630	0.000142	0.000430	110.6	4.0199	103.99	13.16
1075	29.09906	1.22212	0.03221	0.00059	0.0002119	0.000117	0.000542	93.6	2.5624	92.67	11.38
1125	31.46007	0.32618	0.03230	0.00017	-0.0000552	0.000031	0.001931	101.5	27.8701	99.98	3.03
1175	30.01839	0.58478	0.03233	0.00030	0.0001000	0.000055	0.001120	96.9	9.5110	95.52	5.44
1225	21.40458	8.31494	0.03927	0.00606	0.0005397	0.000963	0.000082	83.5	0.5381	68.62	78.47
1275	9.74252	18.80665	0.04261	0.01640	0.0019792	0.002473	0.000036	40.2	0.2275	31.56	181.17
1350	-45.63196	38.96507	0.04024	0.03005	0.0095985	0.008408	0.000019	-186.0	0.1079	-155.64	416.40
1400	-50.24208	49.70293	0.02869	0.02004	0.0082621	0.006970	0.000015	-146.0	0.0990	-172.13	536.03
KP-16 sericite; J = 0.0018016											
700	29.73786	0.40693	0.01030	0.00002	0.0026480	0.000012	0.003895	30.6	1.2438	94.15	3.77
800	32.78763	0.11891	0.02759	0.00005	0.0003644	0.000009	0.005820	90.3	4.9873	103.54	1.09
850	31.85607	0.40953	0.02813	0.00014	0.0003966	0.000035	0.005981	89.5	6.8752	100.68	3.78
900	31.21100	0.05797	0.03048	0.00003	0.0001857	0.000005	0.010932	95.0	15.5049	98.69	0.54
950	30.36276	0.01595	0.03258	0.00001	0.0000416	0.000001	0.063732	98.8	74.0919	96.08	0.15
1000	30.37165	0.01986	0.03271	0.00002	0.0000252	0.000002	0.038970	99.2	51.1837	96.11	0.18
1033	30.31887	0.05428	0.03250	0.00003	0.0000559	0.000005	0.013562	98.4	21.8216	95.95	0.50
1066	30.34331	0.10413	0.03215	0.00006	0.0000934	0.000009	0.006389	97.4	11.8716	96.02	0.96
1100	30.15941	0.14270	0.03222	0.00007	0.0001083	0.000014	0.004861	97.0	8.8991	95.45	1.32
1133	30.33206	0.08385	0.03227	0.00005	0.0000807	0.000007	0.008500	97.8	13.7739	95.99	0.78
1166	30.35387	0.03571	0.03276	0.00002	0.0000218	0.000003	0.018524	99.3	33.5631	96.05	0.33
1200	30.37540	0.05477	0.03265	0.00003	0.0000315	0.000005	0.012743	99.1	22.3387	96.12	0.51
1250	22.18722	2.22048	0.03199	0.00102	0.0011081	0.000216	0.000303	70.5	0.5059	70.71	20.82
1300	3.87129	11.13935	0.03057	0.00476	0.0033651	0.001141	0.000061	10.4	0.1329	12.54	107.86

Appendix B. continued.

Temp (°C)	$^{40}Ar^*/^{39}Ar$	±1σ	$^{39}Ar/^{40}Ar$	±1σ	$^{36}Ar/^{40}Ar$	±1σ	^{39}Ar	$^{40}Ar^*$ (%)	K/Ca	Age (Ma)	±1σ (Ma)
KP-20 biotite; J = 0.0018333											
600	-283.81355	13.84701	-0.01210	0.00134	-0.0066518	0.000632	0.001251	343.9	0.2996	-1325.32	286.42
700	-10.83976	0.58388	0.03079	0.00047	0.0036443	0.000061	0.009698	-33.6	0.9024	-36.21	5.91
800	11.51584	0.22423	0.02571	0.00011	0.0019233	0.000015	0.010086	29.4	1.3834	37.69	2.18
850	25.09176	0.05585	0.02922	0.00002	0.0007288	0.000005	0.022075	73.2	5.4286	81.14	0.53
900	28.33737	0.03049	0.03120	0.00002	0.0003164	0.000002	0.039891	88.3	10.7099	91.37	0.29
950	29.18633	0.02461	0.03186	0.00001	0.0001920	0.000002	0.041241	92.9	13.0053	94.04	0.23
1000	29.37968	0.03135	0.03208	0.00002	0.0001571	0.000002	0.041938	94.1	14.6932	94.64	0.30
1050	29.24078	0.02715	0.03109	0.00001	0.0002488	0.000002	0.055234	90.8	13.9388	94.21	0.26
1100	29.55570	0.02174	0.03201	0.00001	0.0001474	0.000002	0.078782	94.5	15.4622	95.20	0.20
1150	29.33178	0.01676	0.03333	0.00002	0.0000608	0.000001	0.154472	97.7	20.0389	94.49	0.16
1200	29.31091	0.01601	0.03376	0.00002	0.0000283	0.000001	0.182524	98.9	32.7317	94.43	0.15
1300	29.22713	0.13840	0.03206	0.00009	0.0001724	0.000012	0.012774	93.6	6.2926	94.17	1.30
1400	-10.37456	3.80005	0.01731	0.00069	0.0032229	0.000215	0.000555	-18.2	0.5234	-34.64	38.44
KP-12 biotite; J = 0.001825											
600	-16.04812	38.35375	-0.00500	0.00060	0.0031127	0.000611	0.002869	8.2	0.2374	-53.63	390.26
700	-2.00067	0.25806	0.04769	0.00043	0.0037070	0.000039	0.011290	-9.9	0.7892	-6.60	2.56
800	11.06232	0.11170	0.04348	0.00014	0.0017564	0.000013	0.024242	47.9	1.7409	36.06	1.08
850	25.17020	0.53642	0.02922	0.00020	0.0008948	0.000048	0.029399	73.5	8.6486	81.02	5.07
900	30.44761	0.09096	0.02874	0.00005	0.0004228	0.000007	0.037604	87.4	12.1834	97.56	0.85
950	31.85018	0.13448	0.02704	0.00006	0.0004692	0.000010	0.019297	86.0	8.0082	101.93	1.26
1000	32.05995	0.09392	0.02720	0.00004	0.0004327	0.000007	0.020908	87.1	10.5272	102.58	0.88
1050	32.75946	0.17438	0.02667	0.00008	0.0004270	0.000011	0.012266	87.3	9.5245	104.76	1.63
1100	33.06499	0.04087	0.02760	0.00002	0.0002959	0.000003	0.030602	91.2	17.4397	105.71	0.38
1150	32.21137	0.04054	0.02915	0.00002	0.0002063	0.000003	0.025504	93.8	17.2864	103.05	0.38
1200	27.82782	0.54827	0.02869	0.00021	0.0006820	0.000047	0.002450	79.7	1.8655	89.37	5.15
1300	20.22589	1.12199	0.03001	0.00052	0.0013300	0.000100	0.000977	60.4	0.8127	65.39	10.69
1400	-9.70827	5.94590	0.01874	0.00118	0.0039998	0.000378	0.000194	-18.9	0.1842	-32.25	59.79

Appendix B. continued.

Temp (°C)	$^{40}Ar^*/^{39}Ar$	±1σ	$^{39}Ar/^{40}Ar$	±1σ	$^{36}Ar/^{40}Ar$	±1σ	^{39}Ar	$^{40}Ar^*$ (%)	K/Ca	Age (Ma)	±1σ (Ma)
KP-10 biotite; J = 0.0018142											
700	21.20694	0.74634	0.01917	0.00017	0.0020086	0.000039	0.004373	40.6	3.2029	68.11	7.06
800	28.86720	0.10928	0.02979	0.00005	0.0004737	0.000010	0.007145	85.9	9.6445	92.09	1.02
850	29.85220	0.05416	0.03226	0.00003	0.0001249	0.000005	0.014267	96.2	25.8826	95.15	0.50
900	30.18483	0.06239	0.03227	0.00004	0.0000879	0.000006	0.013748	97.3	25.9070	96.18	0.58
950	30.30883	0.07533	0.03212	0.00004	0.0000900	0.000007	0.010244	97.2	22.6066	96.57	0.70
1000	30.68577	0.07899	0.03225	0.00004	0.0000353	0.000007	0.009947	98.9	24.3905	97.74	0.73
1050	31.30342	0.05174	0.03137	0.00002	0.0000613	0.000005	0.016418	98.1	26.0757	99.65	0.48
1100	30.72059	0.02804	0.03228	0.00002	0.0000283	0.000002	0.032006	99.1	40.6536	97.85	0.26
1150	30.36788	0.02470	0.03256	0.00002	0.0000380	0.000002	0.036641	98.8	51.8351	96.75	0.23
1200	30.12964	0.05158	0.03274	0.00003	0.0000461	0.000005	0.016791	98.5	31.9697	96.01	0.48
1300	28.72927	0.42741	0.03146	0.00021	0.0003255	0.000040	0.002088	90.3	5.3648	91.66	3.99
1400	5.52780	8.81054	0.01254	0.00070	0.0031495	0.000349	0.000117	6.6	0.2668	18.00	85.65
KP-25 biotite; J = 0.0018382											
600	-6.23897	1.14955	0.01905	0.00033	0.0037862	0.000061	0.003464	-12.1	0.7256	-20.81	11.57
700	2.14105	0.34114	0.02986	0.00023	0.0031678	0.000031	0.008072	6.2	0.9989	7.09	3.38
800	17.32255	0.12875	0.02914	0.00006	0.0016760	0.000011	0.012243	50.3	1.9574	56.55	1.24
850	26.36667	0.05691	0.03044	0.00003	0.0006680	0.000005	0.019034	80.1	4.8880	85.39	0.54
900	30.37485	0.09459	0.03074	0.00009	0.0002239	0.000002	0.039531	93.3	11.0868	98.02	0.89
950	29.70855	0.02721	0.03189	0.00002	0.0001782	0.000002	0.048683	94.6	14.1242	95.93	0.26
1000	30.19117	0.02406	0.03195	0.00002	0.0001202	0.000002	0.047082	96.3	16.8193	97.44	0.23
1050	30.64907	0.03564	0.03086	0.00003	0.0001832	0.000002	0.054248	94.5	13.5478	98.88	0.34
1100	30.68925	0.03743	0.03110	0.00003	0.0001545	0.000002	0.069050	95.3	12.1464	99.01	0.35
1150	29.99298	0.02069	0.03273	0.00002	0.0000625	0.000001	0.156321	98.0	23.0358	96.82	0.20
1200	29.73055	0.01817	0.03313	0.00002	0.0000510	0.000001	0.110704	98.4	26.4672	95.99	0.17
1300	29.51437	0.11037	0.03220	0.00007	0.0001684	0.000009	0.010601	94.9	7.2364	95.31	1.04
1400	8.49438	2.95598	0.01888	0.00066	0.0028414	0.000172	0.000436	15.7	0.3569	27.95	28.96

Appendix B. continued.

Temp (°C)	$^{40}Ar^*/^{39}Ar$	±1σ	$^{39}Ar/^{40}Ar$	±1σ	$^{36}Ar/^{40}Ar$	±1σ	^{39}Ar	$^{40}Ar^*$ (%)	K/Ca	Age (Ma)	±1σ (Ma)
KP-13 biotite; J = 0.0018216											
700	16.47401	0.68710	0.02409	0.00025	0.0020410	0.000047	0.002067	39.5	1.3401	53.34	6.58
800	24.70826	0.23608	0.03252	0.00014	0.0006645	0.000021	0.004904	80.2	6.0397	79.42	2.23
850	30.84954	0.15417	0.03084	0.00011	0.0001648	0.000011	0.008653	95.0	20.1553	98.63	1.44
900	29.99098	0.06922	0.03269	0.00004	0.0000659	0.000006	0.016340	98.0	42.9635	95.96	0.65
950	30.25209	0.07647	0.03283	0.00004	0.0000235	0.000007	0.013051	99.2	39.0897	96.78	0.71
1000	30.41638	0.09530	0.03269	0.00005	0.0000194	0.000009	0.010527	99.3	46.1024	97.29	0.89
1050	30.81957	0.09382	0.03224	0.00005	0.0000217	0.000009	0.010671	99.3	40.3694	98.54	0.88
1100	30.99294	0.05125	0.03210	0.00003	0.0000175	0.000005	0.020036	99.4	69.1995	99.08	0.48
1150	30.21787	0.02710	0.03295	0.00002	0.0000150	0.000002	0.039492	99.5	137.0630	96.67	0.25
1200	30.14549	0.03251	0.03313	0.00002	0.0000042	0.000003	0.035847	99.8	269.1624	96.44	0.30
1300	30.07516	0.14995	0.03312	0.00009	0.0000131	0.000014	0.007050	99.5	54.0845	96.22	1.40
1400	12.34614	7.12022	0.03308	0.00399	0.0020020	0.000720	0.000158	40.7	1.8809	40.12	68.65
KP-14 biotite; J = 0.0018424											
600	8.59867	13.29741	0.01632	0.00310	0.0029092	0.000501	0.007902	13.9	1.0827	28.36	130.53
700	-4.79702	0.47366	0.03519	0.00039	0.0039554	0.000055	0.007007	-17.3	0.5700	-16.02	4.77
800	23.76668	0.08719	0.03042	0.00005	0.0009371	0.000007	0.022031	72.2	3.1489	77.32	0.83
850	27.06316	0.11493	0.03341	0.00008	0.0003240	0.000010	0.048913	90.3	14.8510	87.78	1.09
900	27.39593	0.01891	0.03574	0.00002	0.0000706	0.000002	0.064784	97.8	30.9307	88.84	0.18
950	27.03559	0.03579	0.03622	0.00003	0.0000707	0.000003	0.033184	97.8	18.4259	87.70	0.34
1000	28.26827	0.05394	0.03456	0.00004	0.0000776	0.000005	0.023842	97.6	14.8385	91.59	0.51
1050	28.22997	0.05134	0.03473	0.00003	0.0000659	0.000005	0.022057	97.9	16.2075	91.47	0.49
1100	28.63182	0.02787	0.03446	0.00002	0.0000451	0.000003	0.042590	98.6	30.0261	92.74	0.26
1150	28.03796	0.01445	0.03541	0.00002	0.0000240	0.000001	0.141687	99.2	103.6677	90.87	0.14
1200	26.50497	0.01855	0.03731	0.00002	0.0000376	0.000002	0.076831	98.8	48.9932	86.01	0.18
1300	24.17572	0.22134	0.03974	0.00020	0.0001325	0.000024	0.006184	95.9	6.1739	78.62	2.11
1400	11.98174	3.05631	0.03706	0.00252	0.0018814	0.000330	0.000510	43.9	0.6136	39.39	29.82

Appendix B. continued.

Temp (°C)	$^{40}Ar^*/^{39}Ar$	±1σ	$^{39}Ar/^{40}Ar$	±1σ	$^{36}Ar/^{40}Ar$	±1σ	^{39}Ar	Age (Ma)	±1σ (Ma)
KP-26 sericite; J = 0.0018128									
700	21.21125	0.70783	0.01387	0.00007	0.0023886	0.000027	1.427E-12	67.97	6.68
800	20.60073	0.32997	0.01346	0.00003	0.0024456	0.000012	2.904E-12	66.05	3.12
900	26.98967	0.10296	0.02125	0.00003	0.0014431	0.000005	1.091E-11	86.05	0.96
1000	26.07326	0.28833	0.01610	0.00004	0.0019635	0.000012	3.623E-12	83.19	2.70
1050	26.68796	1.13663	0.01178	0.00009	0.0023206	0.000038	1.236E-12	85.11	10.62
1100	28.70882	0.83375	0.01826	0.00016	0.0016105	0.000043	2.428E-12	91.39	7.76
1150	31.45076	1.25049	0.01930	0.00028	0.0013296	0.000067	2.333E-12	99.88	11.59
1200	92.29184	15.38270	0.01970	0.00370	-0.0027693	0.001061	2.758E-13	278.69	129.12
1250	412.59964	78.88143	-0.00398	0.00085	0.0089387	0.002129	7.976E-14	1006.29	442.37
1300	384.39289	117.58528	0.00191	0.00034	0.0008982	0.000676	7.044E-14	952.78	679.28
KP-09 biotite; J = 0.0018128									
700	12.45769	0.13410	0.02694	0.00005	0.0022484	0.000011	7.487E-12	40.29	1.29
800	28.96501	0.18338	0.02705	0.00007	0.0007324	0.000013	4.930E-12	92.32	1.71
850	31.84291	0.42981	0.02527	0.00015	0.0006612	0.000026	2.000E-12	101.25	3.99
900	32.77460	0.40406	0.02474	0.00014	0.0006402	0.000024	2.294E-12	104.12	3.74
950	32.30486	0.56993	0.02398	0.00019	0.0007622	0.000033	1.603E-12	102.67	5.28
1000	34.66696	0.40866	0.02425	0.00014	0.0005397	0.000024	2.529E-12	109.96	3.77
1050	33.79652	0.43496	0.02591	0.00017	0.0004204	0.000027	2.865E-12	107.28	4.02
1100	29.96173	4.81906	-0.27938	0.24274	0.0317100	0.027884	3.052E-13	95.42	44.85
1125	40.55259	6.69593	-0.02896	0.00357	0.0073585	0.001067	2.486E-13	127.98	61.20
1150	-47.18991	7.80776	0.00304	0.00005	0.0038698	0.000072	2.884E-13	-161.33	83.77

Notes: Isotopic ratios corrected for blank, radiation decay, mass discrimination, and interfering reactions; individual analyses show analytical error only; plateau and preferred ages on Table 2 include error in J and irradiation parameters; K/Ca = molar ratio calculated from reactor produced $^{39}Ar_K$ and $^{37}Ar_{Ca}$.

APPENDIX C. APATITE LA-ICP-MS FISSION TRACK AND (U-Th)/HE ANALYTICAL DATA.

Sample	Apatite grains (dmnls)	Ns (tracks)	Area analyzed (cm^2)	$\sum(P\Omega)$ (cm^2)	$1\sigma \sum(P\Omega)$ (cm^2)	ξ_{MS}	$1\sigma \xi_{MS}$	^{43}Ca (apatite) blk:sig (dmnls)	^{238}U blk:sig (dmnls)	Q (dmnls)	Pooled Fission Track Age ± σ (Ma)
KP-14	24	593	9.10E-04	5.6212E-05	5.0676E-07	11.3879	0.8094	4.7536E-03	2.6703E-03	0.0075	59.8±4.9

Abbreviations are as follows: Ns = number of spontaneous (fossil) tracks counted; $\sum(P\Omega)$ = sum of the $^{238}U/^{43}Ca$ ratios measured over the Ω area; ξ_{MS} = Zeta calibration factor based on LA-ICP-MS analyses of fission track standards (Durango and Fish Canyon apatite); blk:sig = blank/signal ratio; dmnls = dimensionless quantity; Q = Chi^2 probability.

Sample	Length (µm)	Radius (µm)	Rs (µm)	Mass (µg)	U (ppm)	Th (ppm)	U/Th	He (nmol/g)	Raw Age ± σ (Ma)	Ft	Corrected Age ± σ (Ma)
KP-14 (A)	193.72	95.82	54.45	4.47	29.29	23.65	1.24	6.78	32.64±1.34	0.73	44.65±1.83
KP-14 (B)	168.39	90.12	50.69	3.44	28.03	24.17	1.16	6.30	31.35±1.48	0.71	44.01±2.08

Abbreviations are as follows: Rs = Spherical grain radius; Ft = alpha ejection correction (Farley *et al*., 1996; Farley, 2002).